ABSTRACT

Title of thesis: VISUALIZATION OF THE VORTEX LATTICE DYNAMICS IN SUPERFLUID HELIUM

Kristina T. Gaff, Master of Science, 2010

Thesis directed by: Professor Daniel Lathrop
Department of Physics

We study the lattice structure and dynamics of the quantized vortices in superfluid helium-4 using a new rotating experiment. This setup includes control of the entire apparatus from the rotating frame, installation of a new EMCCD camera that allows for imaging of nanoscale tracer particles, and the development and implementation of a new isolation cell, which permits investigation into new phenomena such as differential rotation in helium-II. We have observed the vortex lattice dynamics in the (r, ϕ) plane (i.e. transverse to the vortices) and present here the first real-time visualization of Tkachenko waves in helium-II from this cross section. Additionally, we present evidence of differential rotation with distinct Stewartson layer boundaries, possible Kelvin-Helmholtz instabilities, and the formation and propagation of superfluid collective vortex eddies. We show that the angular velocity is a function of radius and may be driven by the geometry of the isolation cell. We also document the observation and analysis of gravity-capillary surface waves that demonstrate an interaction between the liquid helium free surface and the bulk of the fluid.

VISUALIZATION OF THE VORTEX LATTICE DYNAMICS IN SUPERFLUID HELIUM

by

Kristina T. Gaff

Thesis submitted to the Faculty of the Graduate School of the
University of Maryland, College Park in partial fulfillment
of the requirements for the degree of
Master of Science
2010

Advisory Committee:
Professor Daniel Lathrop, Chair/Advisor
Professor John Rodgers
Professor Rajarshi Roy

DEDICATION

To my soulmate, Michael.

This story began with a walk in the moonlight.

ACKNOWLEDGMENTS

If there is one section I value more highly than all the others, the Acknowledgments section is it. At times, graduate school has been a muddy, uphill climb, and I would have stayed stuck at the bottom had it not been for a few outstanding individuals who helped me along the way.

First and foremost, I would like to thank my advisor, Dan Lathrop, an energetic physicist who I met during lunchtime bike rides while at Maryland for an REU in 2006. He offered me a spot in his lab before I had even arrived at graduate school and has since shown me how to think of a physics lab more like a toy factory than a workplace.

But if our lab is a toy shop, then Don Martin is the master toymaker. His tireless support and enthusiasm, coupled with his indispensable expertise, advice and ideas, were crucial to my experiments and my daily life.

And what would a lab be without labmates? Enrico, Axl, Matthew, Matt, Doug, Santiago, Kaitlyn, Myung, and Cecilia – thanks for making this lab one of a kind!

Additionally, I would like to thank John Rodgers and Raj Roy for serving on my committee. John has been especially instrumental in my graduate school journey, first as my REU advisor, and then as my friend and mentor for the last four years.

And since I probably would have not graduated on time without her, I simply must add a statement of gratitude for the amazing Jane Hessing who helped me out of more than one predicament in the last several months. She is truly a blessing to the Department of Physics.

Closer to home, I would like to thank my roommates, Caitlin, Kristen, and Cecilia,

for forming the foundation of my physics family for the last two years. From our aspiring neighborhood Mariache band, pet cockroaches, and bedbug infestations to our weekly family dinners, whimsical house rules, and gluten-free baked goods, it has been a memorable ride. To you girls, and to the numerous other classmates, colleagues and friends who I have encountered during my time here at Maryland, thank you; I could not have done it without you.

But it is my family who set the stage for this journey long ago, teaching me first-hand the value of hard work and duct tape, both of which have been invaluable during my burgeoning physics career. They encouraged me to follow my dreams – whatever they may be and wherever they may lead – throughout every step of the way. I hope that, every day, they know how grateful I am.

And last, but only because he is the last thought on my heart and mind every night before I fall asleep, I give my eternal gratitude to my own heart's own, my treasure, my prince – my fiancé, Michael. You didn't just hold my hand and support me, you sang to me a song of the stars and forever reminded me of the Beauty of physics and math – that is why we study it. You are my dream come true, and I cannot wait to marry you.

This research has been generously funded by the National Science Foundation.

TABLE OF CONTENTS

LIST OF FIGURES

LIST OF SYMBOLS AND ABBREVIATIONS

κ	quantum of circulation; 9.97×10^{-4} cm^2/s for superfluid helium
ν, η	viscosity
ρ	fluid density (general)
ρ_n	normal fluid density
ρ_s	superfluid density
ω	angular frequency
Ω	angular frequency of the apparatus
a	helium atom radius
b	mean vortex spacing
h	Planck's constant
$\hbar$	$h/2\pi$
^{4}He	helium-4 isotope
He I	classical fluid state of helium-4
He II	quantum fluid state of helium-4
k_z	longitudinal wavenumber for a bounded system
$\mathbf{l}$	discrete wavevector with radial and azimuthal components (l_r, l_ϕ)
l_r	radial wavenumber
l_ϕ	azimuthal wavenumber
L_z	total angular momentum
l_z	specific angular momentum
p	pressure
$\mathbf{u}$	fluid velocity
$\mathbf{v}_n$	velocity of the normal fluid component
$\mathbf{v}_s$	velocity of the superfluid component

Chapter 1

Introduction and Review

Even after a century of fervent research, the study of superfluid helium remains one of the most enigmatic and fruitful areas of science. This extraordinary substance possesses no viscosity, no entropy, and the highest thermal conductivity of any known material. Moreover, it is one of the few substances through which we can observe quantum mechanical phenomena with our naked eyes. It possesses atomically thin line-like tornadoes called quantum vortices that stretch from wall to wall or end on themselves to form rings, which dictate the relative order of the system. These vortices interact, sometimes by exchanging tails and catapulting off in opposite directions, sometimes by aligning themselves in a lattice-like structure in response to rotation, and still other times by some whimsical combination of nature's most intriguing phenomena including differential rotation and inertial waves. All of this, and it only exists at temperatures colder than that of deep space.

The purpose of this thesis is to explore the story of superfluid helium, particularly the tale it tells when we rotate a vat of it. In the rest of Chapter 1, we set the stage for our studies, elucidating the rich history and theoretical background of superfluid helium that prompted the experiments we pursued. Then, with the background and context established, we describe the experimental apparatus and procedure that we used to conduct our studies in Chapter 2. Chapter 3 follows with our observations and

preliminary analysis, and Chapter 4 closes with our conclusions and ideas for future work. Appendix A includes the first formalized Standard Operating Procedures for the helium experiments in our lab, while Appendix B provides some useful information for the next generation of "super"-helium experimentalists. (This last section contains proprietary information and has been omitted in the online version of this thesis.)

All of the work presented here is that solely of the author unless otherwise noted. In particular, the author would like the acknowledge the contribution of her predecessors, Matthew Paoletti and Gregory Bewley. Greg originally brought the helium experiments to the University of Maryland and was the inventor of the visualization technique we utilize here. Matt purchased and setup the Oxford OptistatSXM cryostat, as well as developed the basic injection and temperature control protocols used below. The rest of the apparatus has been heavily modified or rebuilt to accommodate a fully rotating system (including the camera in the rotating frame) by the author. The rotating table components were designed and built solely by the author under the supervision of senior technician, Don Martin with the exception of the isolation cell (see Figure 2.4 on page 34), which was designed by the author and built jointly by Don Martin and the author owing to time constraints. Additionally, the author researched camera options leading up to the Princeton Instruments ProEM camera that was instrumental in the discovery of the "nanoparticles" discussed in section 2.3.1. The data analysis was done jointly by the author and her advisor Daniel Lathrop, with occasional assistance from fellow lab member Enrico Fonda.

1.1 The Super Fluid

On July 10, 1908, Heike Kamerlingh Onnes, a Dutch physicist particularly enchanted by the allure of ultra-low temperatures, and his team of advanced chemists, instrument makers, glass blowers, and "blue-collar boys[1]," won the cold war on liquid helium (see Fig. 1.1). Helium was the last "permanent gas" to be liquefied, and utilizing an elaborate setup of liquid hydrogen and the Joule-Thomson effect (whereby gas is adiabatically expanded and cooled), Onnes produced 60 mL (2 fluid ounces) of liquid helium – barely enough to fill a small teacup, but more than enough to earn him a Nobel prize five years later in 1913[2] [1]. By further exploiting the Joule-Thomson effect, Onnes and his team were later able to cool the liquid helium to 0.9 K, less than one degree above absolute zero, making Leiden, The Netherlands home to the coldest place on earth in the early twentieth century [2, 3]

For the next 15 years, no other lab possessed the equipment and expertise needed to replicate Onnes' liquefaction experiments. It was not until John McLennan traded a few cylinders of valuable helium gas in exchange for technical drawings and advice from Onnes that the University of Toronto stepped into the liquid helium scene. This lab would go on to train some of the most innovative and brilliant minds in liquid helium research, including Jack Allen and Don Misener, but even so, Leiden would still be home to the next major revelation in the helium revolution.

In the mid-1920s, Onnes had remarked as to the volatility of helium around 2.2

[1] students from the neighboring School for Instrument Makers

[2] The fact that Onnes used liquid helium to cool mercury enough that its resistance fell to zero, thus discovering the first superconductor in 1911 [4] did not go unnoticed. However, while these events were indubitably excellent for the advancement of science, they had the unfortunate side effect of relegating liquid helium to that of a mere coolant for nearly two decades.

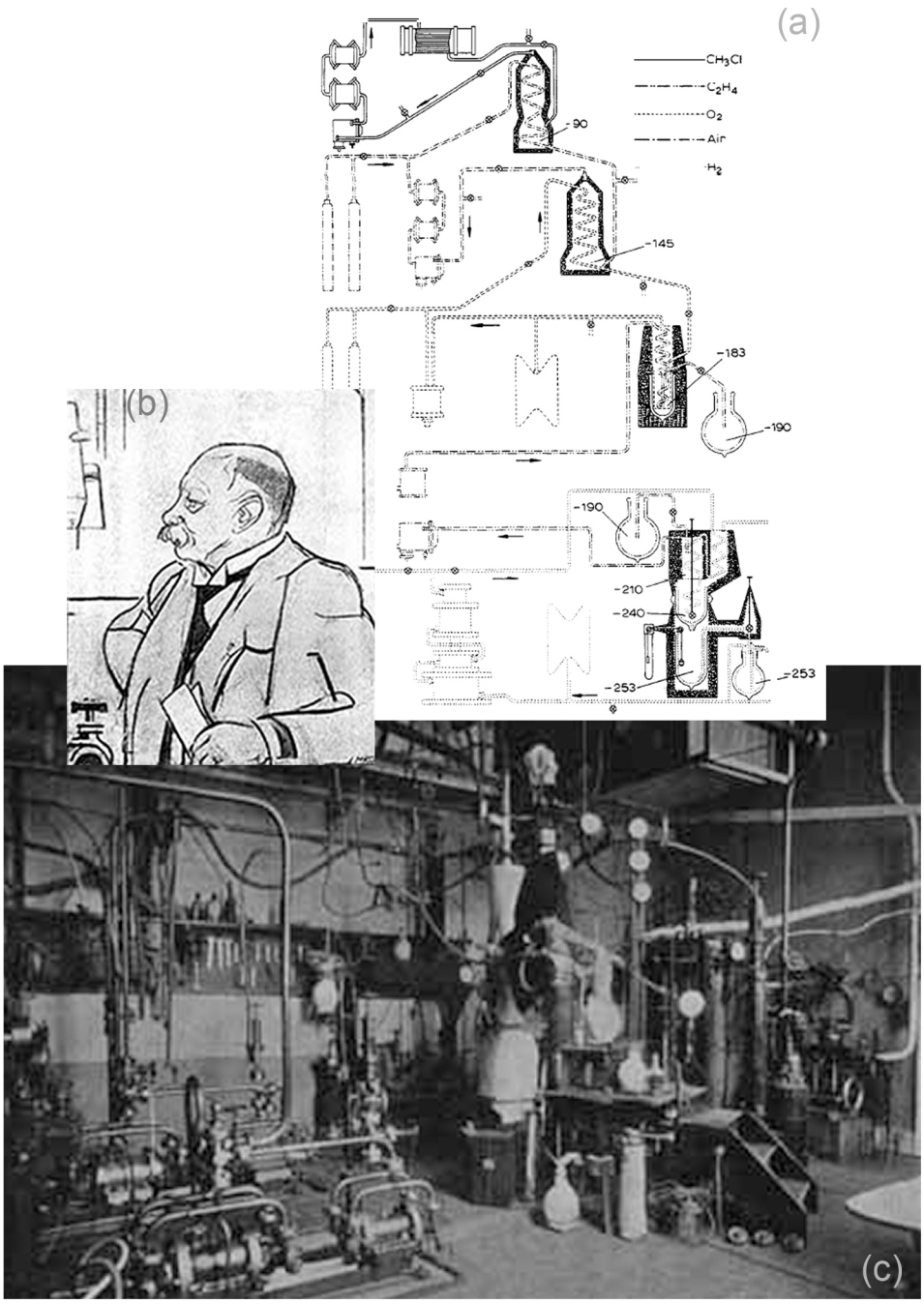

Figure 1.1: (a) Schematic from Onnes' Nobel prize lecture depicting the liquefying process. Note that hydrogen was first cooled using liquid air, then the liquid hydrogen was iteratively pumped through the Hampson-Linde process to cool helium gas to 4 K. (c) Photo of the Heike Kamerlingh Onnes Laboratory showing a substantial portion of helium liquefying apparatus from the American Institute of Physics Emilio Segre Visual Archives, Brittle Books Collection. (b) Self-portrait of H. K. Onnes from the same collection.

K, even publishing that the helium density was a maximum $\sim$2.18 K [6]. He knew this fact was perhaps indicative of a phase transition, but he was also known to be a stickler for precise data[3], and he was hesitant to make any further claims. It was not until after his death that one of Onnes' assistants, Willem Keesom, and visiting Polish physicist Mieczyslaw Wolfke officially announced that liquid helium possessed two different states of matter. They dubbed the liquid helium above 2.18 K "helium I" and the liquid below that temperature "helium II" [7, 8, 9]. A few years later, in 1930, Keesom and J. N. van der Ende noticed that helium-II (He II) flowed seemingly effortlessly through the tiniest of pores [10]. Two years later, Keesom and his colleague K. Clusius published the specific heat curve for liquid helium, which showed an unambiguous anomaly at the transition between the helium-I and helium-II states (see Fig. 1.2) [11]. Keesom performed similar measurements with his then 17-year-old daughter Anna Patronella, who titled[4] the transition the "λ-transition" owing to its likeness to the Greek letter [12, 13]. That same year, McLennan and his team in Canada (H. D. Smith and J. O. Wilhelm) discovered that liquid helium appeared to stop boiling below this so-called λ-transition temperature, T_λ (see Fig. 1.3). (This phenomenon would later be explained by both Allen, Peierls, and Uddin of Cambridge [20] and Keesom and his daughter [19] as a result of the high thermal conductivity of He II.) In 1933, Keesom wrote that there was no latent heat associated with the λ-transition, making it a continuous, or second-order, phase transition [15]. This fact put helium-II in the same family as ferromagnetics, superconductors, and liquid crystals. In fact, the latter two of these

[3] A dedicated experimentalist, Onnes' personal motto was, "Knowledge through Measurement" (*Door meten tot weten*).

[4] after a suggestion by head-of-department, Paul Ehrenfest.

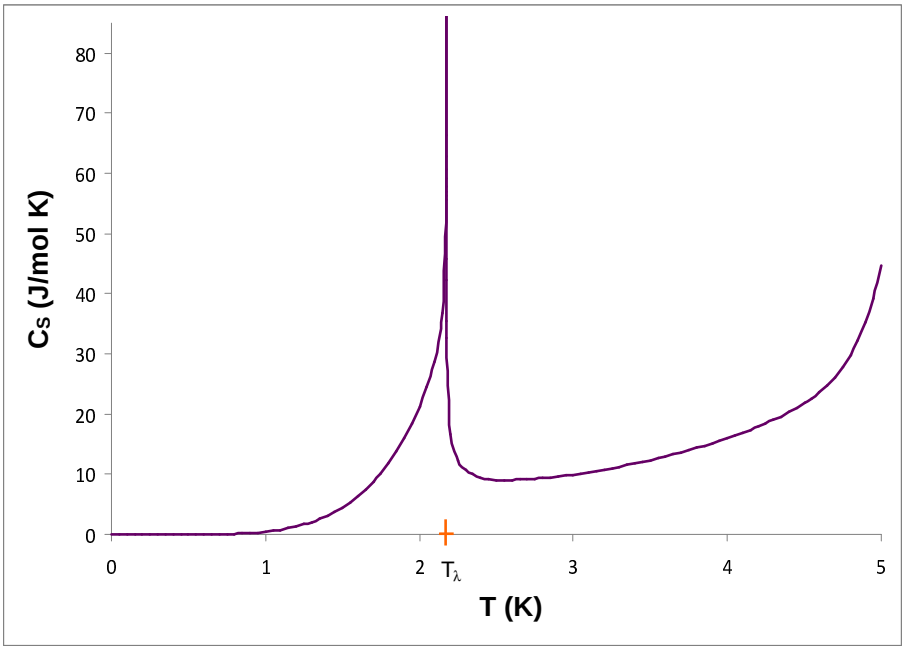

Figure 1.2: Specific heat curve for liquid helium at low temperatures and saturated vapor pressure. Plot generated by the author with data from [22].

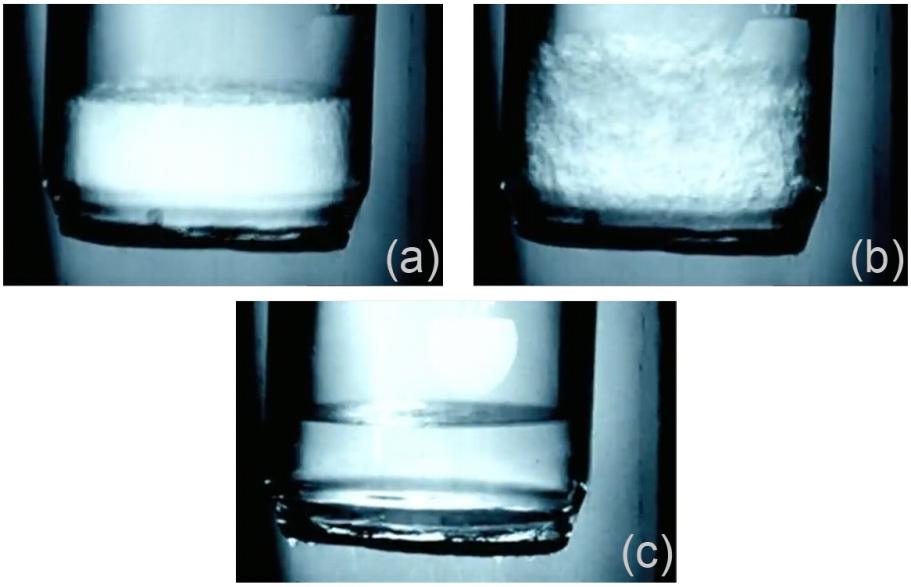

Figure 1.3: (clockwise from left) As liquid helium is cooled, one observes typical fluid boiling above transition ($T > T_\lambda$), violent boiling around transition ($T = T_\lambda$), and no visible boiling below transition ($T < T_\lambda$). This peculiarity is a consequence of the ballistic heat transport of the superfluid. Images adapted from [21].

examples are also members of the λ-transition universality class because of their many similarities, including their formalisms, topological defects, and typical phase diagrams.

Then, in 1935, the Toronto team of Wilhelm, Misener, and Clark[5] set out to determine the viscosity of He II by measuring the decay rate of a cylinder executing torsional oscillations while immersed in a bath of liquid helium [16, 17]. While these measurements showed that the viscosity decreased sharply below T_λ, some argued that the results were inconclusive owing to the possibility of turbulent motion. So Misener left Toronto to join Jack Allen in Cambridge and together they studied more closely the flow rate of liquid helium in very small capillary tubes. They knew that, classically, fluids followed Poiseuille's Law for laminar pipe flows. That is, the rate of flow, $\mathfrak{f}$, of a Newtonian incompressible fluid through a capillary tube is proportional to the fourth power of the tube's radius such that

$$\mathfrak{f} = \frac{\pi(\Delta p) r^4}{8\eta L}$$

where L is the tube length, ν is the viscosity, Δp is the pressure difference between the ends of the tube, and r is the tube radius. Yet, Allen and Misener – and independently Pyotr Kapitsa in Russia – did not find this relationship. Instead, they found that the flow was *independent* of both pressure and radius. The liquid helium below 2.18 K seemed to flow without any resistance at all! The two groups published pivotal back-to-back papers in *Nature* in January of 1938 [23, 24]. Just like Onnes had found the resistance of mercury to vanish when he discovered superconductivity, Allen, Misener, and Kapitsa had found the viscosity (the "resistance to flow") to be immeasurably low. Befittingly,

[5]Wilhelm operated the helium liquefier, Misener led the experiment, and Clark was the senior technician [18].

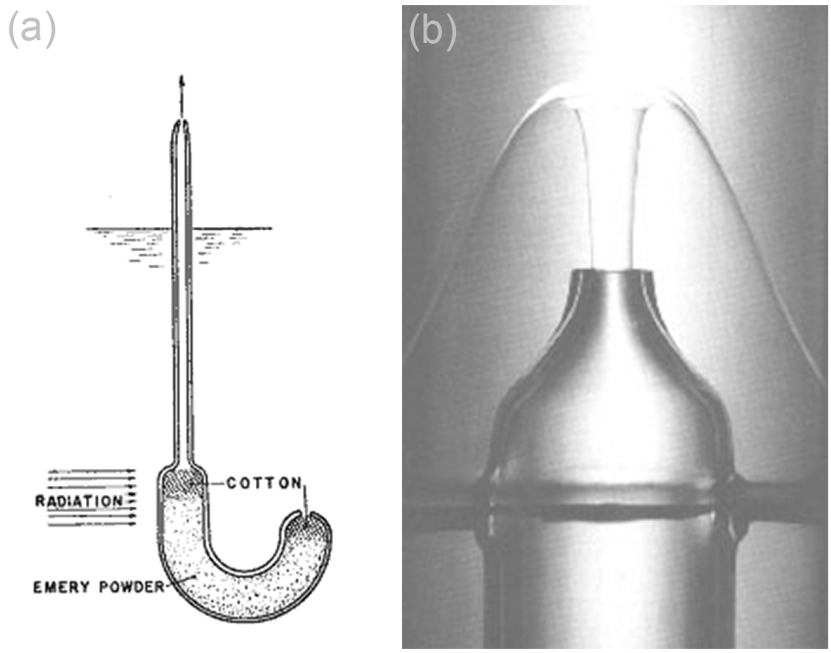

Figure 1.4: (a) Schematic of experimental apparatus used to produce the "fountain effect" by Allen and Jones [25]. The superfluid component of helium-II always flows toward any source of heat. Hence, by illuminating the thin tube, the superfluid migrates toward the heat source, decreasing its mass density in the surrounding fluid and inducing a pressure gradient, which propels it up the tube. The image on the right, from [26], depicts the spectacle in action.

Kapitsa termed this fluid a "superfluid."

The research only accelerated from this point. Experimentally, Allen, colleague H. Jones, and (although not an author of the resulting paper) Misener discovered a mechanical superfluid response to an influx of thermal energy [25]. When heating a long thin tube partially immersed in a bath of helium-II (see Fig. 1.4), they observed a spurt of liquid helium flowing out the top of the tube. Explaining this thermomechanical effect (also called the "fountain effect") prompted one of the first major theoretical breakthroughs in superfluid helium research: the two-fluid model.

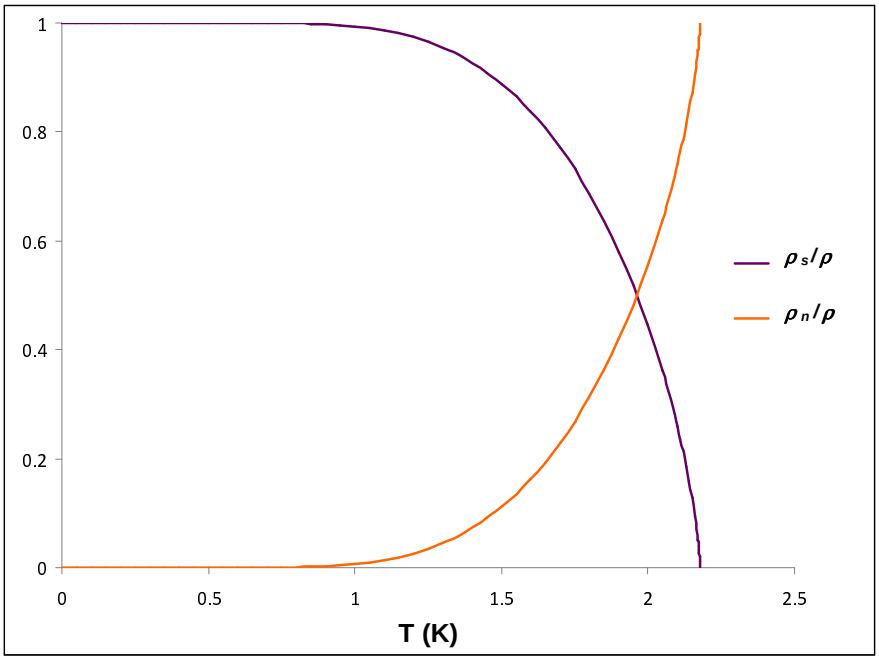

Figure 1.5: Measurements of the normal fluid density and superfluid density of helium-II as a function of temperature at saturated vapor pressure. This plot agrees well with Landau's prediction of the two-fluid model from 1941. Plot generated using data compiled by Donnelly and Barenghi in [22].

1.2 The Two-Fluid Model

Around the same time the researchers in Cambridge were making fountains out of 2 K helium, László Tisza suggested that helium be thought of as a mixture of two fluids: a superfluid constituent, which possesses no viscosity and carries no entropy, and a normal fluid counterpart described as a standard Newtonian fluid [29]. As the temperature decreases from T_λ to $T = 0$, the relative superfluid density increases while the complementary normal fluid density decreases (see Fig. 1.5). With this theory, Tisza explained that it was only the superfluid component that passed through a fine capillary or tiny pores; the normal fluid component would be hindered by its viscous drag. The fountain effect is simply this curiosity in reverse. A temperature gradient prompts a

change in the density of the superfluid, which gives rise to a pressure gradient that drives the superfluid up and out of the tube into a spectacular fountain. In addition, since the superfluid component has no entropy, it leaves behind its heat in the surrounding bath as it exits the tube. This last feature is called the mechano-caloric effect and was first demonstrated by Daunt and Mendelssohn in 1939 [30].

A few years later, Lev Landau developed the two-fluid model more formally in terms of the hydrodynamic equations. In essence, he added a superfluid degree of freedom to the standard set of fluid equations. For example, in his model the total density for helium-II (which is relatively constant) becomes

$$\rho = \rho_s + \rho_n \tag{1.1}$$

where $\rho_n = \rho$ and $\rho_s = 0$ at $T = T_\lambda$ and $\rho_n = 0$ and $\rho_s = \rho$ at $T = 0$. (Note that it is only here, at absolute zero, that the whole of helium-II is a true superfluid.) The normal and superfluid components have distinct velocity profiles as well. Hence, we have a mass flux

$$\mathbf{j} = \rho_n \mathbf{v}_n + \rho_s \mathbf{v}_s \tag{1.2}$$

where $\mathbf{v}_n$ and $\mathbf{v}_s$ are the normal and superfluid component velocities respectively, which follows from the continuity equation

$$\nabla \cdot \mathbf{j} = -\frac{\partial \rho}{\partial t} \tag{1.3}$$

Moreover, the superfluid flow is irrotational:

$$\nabla \times \mathbf{v}_s = 0 \tag{1.4}$$

The significance of this flow will be discussed shortly.

Using these modified forms, we can write the simplest variation of the two-fluid equations as

$$\rho_s \frac{d\mathbf{v}_s}{dt} = -\frac{\rho_s}{\rho}\nabla p + \rho_s S \nabla T + \frac{\rho_n \rho_s}{2\rho}\nabla(\mathbf{v}_n - \mathbf{v}_s)^2 - \mathbf{F}_{ns} \tag{1.5}$$

and

$$\rho_n \frac{d\mathbf{v}_n}{dt} = -\frac{\rho_n}{\rho}\nabla p + \rho_s S \nabla T + \frac{\rho_n \rho_s}{2\rho}\nabla(\mathbf{v}_n - \mathbf{v}_s)^2 - \mathbf{F}_{ns} + \eta\nabla^2\mathbf{v}_n \tag{1.6}$$

where S is the entropy, T is the temperature, η is the viscosity of the normal fluid (the superfluid's viscosity is zero, of course), and $\mathbf{F}_{ns}$ is the mutual friction term [32]. Mutual friction describes the non-negligible interaction of the normal and superfluid components (via the vortex lines) in liquid helium.

Since the superfluid flow is irrotational, it will remain stationary below some critical rotational velocity. The absence of viscosity allows rotation without boundary interaction (i.e. slipping). Above the critical velocity, however, the superfluid flows with quantized circulation, as postulated by Onsager and described below.

1.3 Quantized Vortices

In 1949, Lars Onsager announced that the hydrodynamic circulation for superfluid helium was quantized with quantum of circulation given by $\kappa = h/m$, Planck's constant divided by the mass of a helium atom. He never published this bold proclamation, but it laid the foundation for the quantum mechanical description of helium-II. In 1954, Onsager showed that since the superfluid component has an inviscid flow that is irrotational

(Eq. 1.4), its velocity, v_s, can be described by the gradient of a scalar such that

$$v_s = \nabla\phi \tag{1.7}$$

Then, by Stokes' Theorem, we see that the circulation, given by the line integral of the velocity

$$\Gamma = \oint_C \mathbf{v}_s \cdot d\mathbf{l} \tag{1.8}$$

vanishes over any simply connected region. However, topological defects inside the integration contour can give non-zero contributions to the integral. The possible values of Γ are then some constant multiplied by the winding number of the curve C. In particular, Onsager suggested that the superfluid formed phase defects, or vortices, which carry angular momentum and lead to non-zero circulation. The quantization of circulation is given by the canonical quantization of angular momentum $\kappa = \frac{h}{m}$, so we obtain

$$\Gamma = \oint_C \mathbf{v}_s \cdot d\mathbf{l} = n\kappa \tag{1.9}$$

Assuming rotational symmetry, we find an azimuthal velocity of

$$v_\phi = \frac{\kappa n}{2\pi r} \tag{1.10}$$

where n is the quantization number.

Quantized vortices exist only in superfluids or superfluid-like systems such as liquid helium, Bose-Einstein condensates [40], type-II superconductors [41], liquid crystals [43], the inner cores of neutron stars [56], and perhaps cosmic strings in the early universe [42]. In type-II superconductors, the creation and dynamics of the vortices can

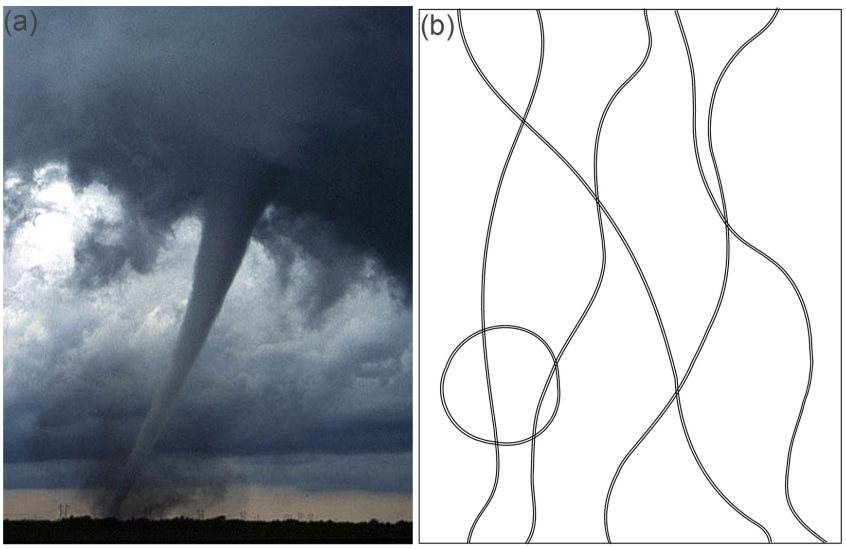

Figure 1.6: A classical vortex, like the tornado seen in (a) from [36], terminates in the fluid (the atmosphere) owing to dissipation by viscous drag. A quantum vortex, on the other hand, is not diffusely spread by viscosity and therefore must either end at the walls, the boundary of the fluid, or on itself as seen in (b).

lead to the breakdown of superconductivity; yet, the opacity of solid superconductors hampers direct observation of these effects except at the edges of the material. In liquid helium, opacity is obviously less of a hindrance; however, the size of these vortices is on the order of that of a helium atom ($\sim$0.1 nm), so they are nominally invisible. Nevertheless, as the methods in Chapter 2 elucidate, it is possible with great care and ingenuity to visualize these vortices with our naked eyes.

1.4 Rotating Helium-II and the Vortex Lattice Array

The first experimental evidence for the existence of quantized vortices in helium-II came through indirect measurements by Hall and Vinen in 1956 [44]. The impetus for their experiment stemmed from Richard Feynman's theoretical analysis of quantized vortices a year prior. Feynman showed that although the superfluid is irrotational (Eq.

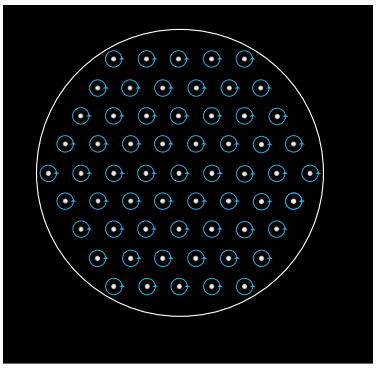

Figure 1.7: Schematic of the quantized vortex lattice array in a rotating cylindrical vessel of liquid helium along the axis of rotation.

1.4) and therefore cannot achieve solid body rotation ($\nabla \times \mathbf{v} = 2\Omega\hat{z}$), the fluid can approximate solid body rotation by forming a lattice with a large number of vortices at nearly uniform density. The optimal configuration for these criteria, and the solution that minimizes energy, is a triangular lattice array (see Fig. 1.7).

Feynman gave a vortex number density approximation of

$$n_0 = \frac{|\nabla \times \mathbf{v}_{lattice}|}{\kappa} \approx \frac{2\Omega}{\kappa} \tag{1.11}$$

where Ω is the rotation rate of the vessel. Thus, approximating κ as $\sim 10^{-3}$, we should see about 2000 lines/cm^2 for a vessel rotating at 1 rad/s or a vortex line approximately every 0.2 mm. The nearest neighbor spacing, d_{NN}, is given by the inverse square root of the line density:

$$d_{NN} = \sqrt{\frac{\kappa}{2\Omega}} \tag{1.12}$$

Although Feynman predicted the triangular lattice in 1955, direct observation of the lattice in helium-II would not occur for nearly two decades. In 1974, Williams and Packard [37] observed a disordered array of vortices whose nearest neighbor spacing did in fact decrease with an increased rotation rate, but which did not adhere to Feynman or-

dered triangular lattice prediction. Then, in 1979, Yarmchuk, Gordon, and Packard [38] captured a lattice array of up to eleven vortices by accelerating electrons, presumably attached to vortex lines, toward a phosphor screen near the free surface. Their lattice array, albeit quite small, agreed well with Feynman's prediction, but they benefitted from temporal averaging, which minimized the effects of any lattice oscillations or stochastic distortions. In 2006, Bewley [39] observed numerous vortex line lengths edge-on (i.e. perpendicular to the axis of rotation), thereby motivating the rotating experiments that form the foundation of this thesis.

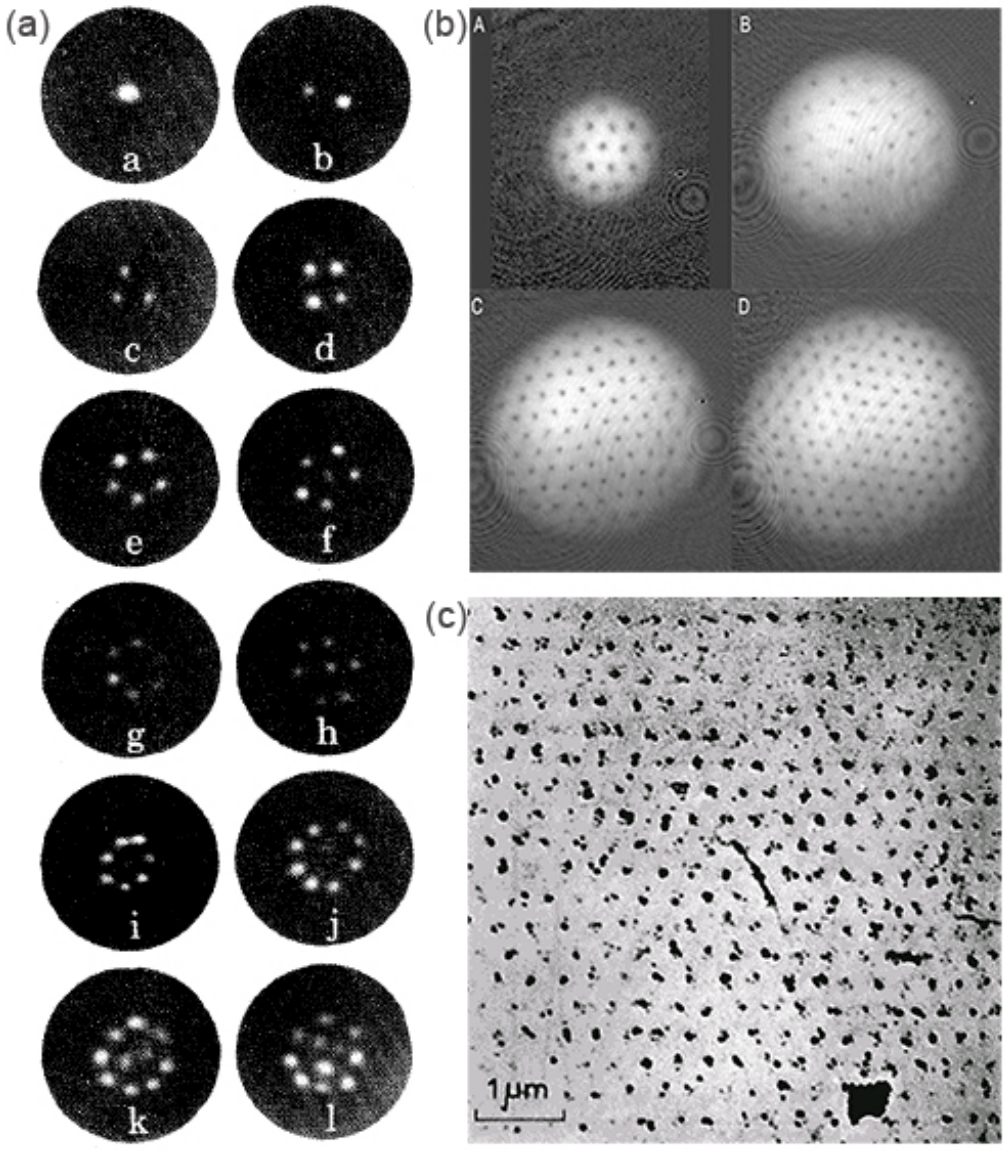

Figure 1.8: Direct observation of the vortex lattice array in (a) helium-4 by [38], (b) Bose-Einstein condensates by [40], and (c) type-II superconductors by [41]. In (a) the tracer particles were ions that were accelerated onto a phosphor screen located at the free surface of the fluid. While this process indeed captures a lattice of up to 11 vortices, showed here for increasing rotation rates (image *a* through *l*), it does not capture the dynamics of the fluid.

Chapter 2

Experimental Design and Procedure

With the theoretical groundwork established, we now delve into how one can actually witness these phenomena. In particular, this chapter describes the major instruments used in our observations including the cryostat, the rotary vacuum unit, the motor and other rotation equipment, the low-light, high-sensitivity camera, the optics, the particle injection technique, and the isolation cell. In addition, it briefly describes the implementation of these devices for the purposes of the data presented here. Detailed operating procedures developed by the author for these experiments are presented in Appendix A.

2.1 The Cryostat

The crux of the entire apparatus is a blue Oxford Instruments OptistatSXM cryostat, which is comprised of three major sections: the liquid helium reservoir or "bath section," the test section, and the surrounding vacuum jacket (see Fig. 2.1). The reservoir stores up to four liters of liquid helium which can then be slowly transferred to the test section via a capillary needle valve when needed. The test section is a 49 mm (1.93 in) cylinder with an effective test height (bottom test section window to top vacuum jacket flange) of 546 mm. It sits at the heart of the cryostat and is equipped with a built-in heater and wall-mounted temperature sensor utilizing Oxford Instruments'

Intelligent Temperature Controller (ITC) technology. The entire test section and reservoir is surrounded by a copper radiation shield. Additional components, such as the injection tube (see Section 2.3.1) and isolation cell (see Section 2.4) can be inserted into the cryostat through a NW50 flange located at the top of the test section space. When the system is at atmospheric pressure (i.e. $T \geq 4.2$ K), these components can be exchanged with relative ease.

To cool the liquid helium below 4.2 K, the system must be sealed and then evaporatively cooled using a mechanical roughing pump connected to the reservoir and test section pumping ports at the top of the cryostat. The partial pressure of the helium bath – and thus, the cooling rate – is modulated by a computer-controlled pneumatic valve. If at any time the test section becomes empty or the liquid helium level becomes too low, it can easily be refilled by opening the needle valve to the reservoir. A faster flow rate can be encouraged by weakly pumping on the test section (see Appendix A for more details). Both the reservoir and the test section are designed to operate at temperatures between 1.6 K and 300 K (room temperature), but the experimentation discussed here generally occurs between 1.7 and 2.2 K.

In addition to these standard cryogenic features, the test section provides generous optical access with four orthogonal radial windows and one axial window. Indeed, the cryostat was originally purchased for this axial window: its position underneath the cryostat allows us to directly visualize the real-time, dynamic motion of the fluid along the axis of rotation – a first in liquid helium history. Each window is 15 mm in diameter and are located 78 mm from the test section bottom. The four radial windows have f2.2 optical access.

Figure 2.1: Cutaway of the Oxford Instruments OptistatSXM used in these experiments. The bulk of the cryostat is a liquid helium reservoir, while the central cylinder is the main testing space for the experiments. A vacuum chamber thermally insulates the entire unit. Image acquired from Oxford Instruments.

The entire system is insulated by an outer vacuum chamber (OVC) or vacuum jacket. This jacket, which is touted to decrease excess vibrations, replaces the need for a nitrogen reservoir.

2.2 Rotating Equipment

While the previous helium experiments in this lab were designed in part for rotation, this setup is the first that rotates the entire apparatus, including the laser, optics, cryostat, computer, and camera along the axis of rotation, all while being able to control the temperature using vacuum pumps which must reside in the lab frame. Additionally, two 120 V AC power lines were routed under the air bearing and wired through the slip ring to supply power from the lab frame to the rotating system. All of the components described here were designed and built by the author (under the supervision of technician Don Martin) unless otherwise noted.

To achieve rotating system *in toto*, the 8' $\times$ 4' optical table was lowered and situated on I-beams six inches off the ground in order to accommodate the extra vertical space necessary so that the camera and equipment could be aligned in $\hat{z}$. The half-ton capacity air bearing was then secured directly to the optical table and a collar was constructed so that a Merotac Model 830 slip ring could rest in the 3" hole in the center of the air bearing. Four sets of wires were soldered to each side of the slip ring: two sets supply 120 V AC power as described above, one set allows for computer control of the pneumatic valve voltage, and the other set provides access to the motor settings. A 24" $\times$ 36" aluminum connector plate was then machined to accommodate

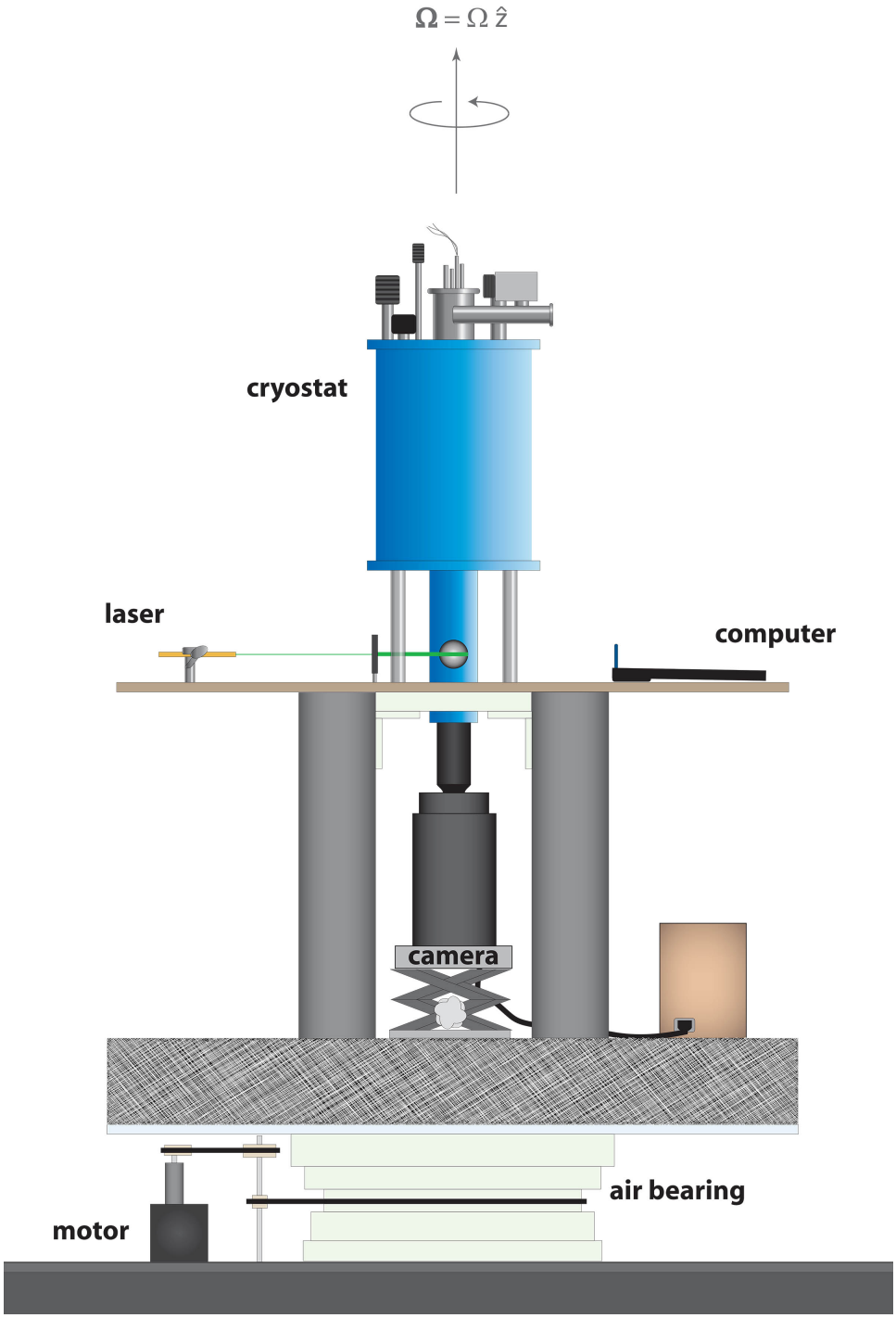

Figure 2.2: Drawing of the experimental setup. The entire apparatus – cryostat, camera, computer, temperature and level sensing equipment, optics, and power supplies – rotates uniformly with $\Omega = \Omega\hat{z}$.

the wires and then attached to the air bearing, creating a platform onto which the 24" $\times$ 36" $\times$ 4" honeycomb damped optical breadboard[1] could be secured with a flush connection. Three 4" $\times$ 4" $\times$ 24" hollow steel beams were then situated uniformly around the center of this optical table, thereby creating space for the camera and its mount to sit comfortably underneath, aligned with the axis of rotation ($\Omega = \Omega\hat{z}$). A 1" thick slab of aluminum was placed on top of the beams, providing a sturdy surface for the steel experimental platform; long threaded rods secured the beams in place. The experimental platform, built by lab member Matt Paoletti for previous experiments (see [34]), supports the optical setup, mixture bottle, cryostat supports, and computer monitor.

Connected to the lid of the cryostat is a rotary vacuum unit. A specially designed collar anchors it in the rotating frame directly above the axis of rotation while it is allowed to rotate freely in the lab frame. This crucial mechanism enables us to control the temperature (via the pressure) of the system using lab-frame pumps and valves, even while rotating the rest of the apparatus.

Lastly, the entire apparatus is rotated uniformly by a 90 V gear-reduction DC motor that has been bolted to the large optical table in the lab frame. It is powered by a 120 V Electronic Motors Inc. (EMI) DC power supply and is then finely tuned with a computer by means of the slip ring wires or by hand using a lab-frame variable voltage power supply. (The latter alternative was employed during many of the runs presented here owing to a short in the slip ring connectors.) The air bearing has an integral toothed gear that is coupled to the motor shaft pulley via an idler shaft and two trapezoidal tooth

[1] henceforth known as the rotating optical table

urethane timing belts. This configuration results in nearly a 6:1 gearing ratio. The low-voltage parameter regime of the motor and power supply necessitate that this ratio be kept as large as possible.

2.3 Visualization Tools and Methods

To capture the dynamics of superfluid helium, we employ a method of particle tracking using hydrogen ice particles developed previously in this lab by Greg Bewley (see [33]). His technique – modified for the new parameter regime of this experiment – enables us to capture movies of the real-time dynamics in He II, as we will discuss further in this section. We will also describe the other essential components for visualization, such as the optical setup, laser, and state-of-the-art camera.

2.3.1 Injection Technique

Traditional Method

As mentioned, the essence of our visualization method rests with gases that freeze at liquid helium temperatures, creating tiny solid particles. Light is scattered off of these particles and captured on camera. For most of the experiments here, we used hydrogen gas, but compositions involving atmospheric gas and propane were also investigated. Details of these latter instances are described more thoroughly under the "New Tiny Particles" heading.

Traditionally (after [33] and [34]), a dilute, room temperature mixture of hydrogen and helium gas is created and stored in a small pressure tank bottle (for more detailed information, see the Standard Operating Procedures in A.2). The bottle is set to a

positive pressure of 15 psi. Then, a computer controlled interface modulates a solenoid valve. When the valve is open, the pressure exchange propels the mixture from the bottle, through 1/8" copper tubing, down the quarter-inch thin-walled stainless steel injection tube, and into the waiting bath of liquid helium. Pure hydrogen freezes at 14 K, so as the mixture travels through the cryostat test section space, the hydrogen particles cool, condense, and then freeze while the helium liquefies at 4.2 K. Since solid hydrogen has a higher index of refraction than the surrounding liquid helium, incoming laser light (see 2.3.2) scatters off of the H_2 ice and is captured by the EMCCD camera. This process is the primary mechanism for visualization of the helium flows in our experiment.

Two needle valves in series with the copper tubing allow for adjustment of the mixture flow rate, while the injection length is a function of the solenoid valve open time. The solenoid valve mechanical response time sets the lower bound for the injection time at 5 ms. During the experimentation phase, injection times of 0.005 - 10 seconds were tested; however most of the results presented here had 0.1 - 3 seconds of injection. This injection time was highly dependent on the dilution of the current mixture: see Chapter 3 for further details pertaining to individual runs.

Particle Trapping

Once the particles are in the liquid helium, they follow a trapping mechanism first outlined by R. J. Donnelly in 1965 [50]. Surrounding each vortex is a dynamic pressure, P, given by

$$P = \frac{1}{2}\rho v^2 \tag{2.1}$$

where ρ is the fluid density and v is the fluid velocity. If we consider the fluid circulating around every vortex to be purely superfluid, then $\rho \to \rho_s$ and $v \to v_s$. Substituting in the superfluid velocity from (1.10), we obtain

$$P = -\frac{\rho_s \kappa^2}{8\pi^2 r^2} \tag{2.2}$$

where $\kappa = {}^{h}/_{m}$ and r is the radial distance from the vortex core. This pressure gives rise to a radial pressure gradient,

$$\frac{dp}{dr} = \frac{\rho_s v_s^2}{r} = \frac{\rho_s \kappa^2}{4\pi^2 r^3} \tag{2.3}$$

which grows as we approach the vortex core. In essence, when acting on a particle with volume V, we have an attractive normal force[2]:

$$\mathbf{F}_{trap} = \int \nabla P \, dV = -\frac{\rho_s \kappa^2}{4\pi^2 r^3} V \, \hat{r} \tag{2.4}$$

pulling the particle onto the vortex core and trapping it there.

The trapping pressure gradient can equally be thought of as a change in the energy density of the fluid, i.e.

$$P = \frac{Force}{Area} \cdot \frac{distance}{distance} = \frac{Energy}{Volume}$$

which can also be seen by comparing Eq. 2.1 to the form for kinetic energy. Then from Bernoulli's equation for stationary height, we have

$$P + \frac{1}{2}\rho v^2 = constant$$

[2]This relationship falls out of Gauss Theorem whereby $\int \nabla \cdot P \, dV = \oint P \cdot \hat{n} \, dA$.

where P is the pressure energy defined above and $\frac{1}{2}\rho v^2$ is the kinetic energy density of the fluid. Consequently, as the pressure density increases (as we approach the vortex core), the kinetic energy density decreases, making it energetically favorable for the particles to be trapped on the vortices. The primary reason for the particles to leave the vortex core is if they are dislodged by the viscous drag (Stokes' drag) of the normal fluid component, which scales linearly with particle size. Thus, it is to our scientific and experimental advantage to produce the smallest particles possible in order to best visualize the true dynamics of the superfluid vortices in He II.

New Tiny Particles

With a little bit of ironic luck, very small particles happened to produce themselves, serving as a catalyst for further experimentation to create consistently puny particles. Soon after installing the new highly-sensitive EMCCD camera (see Section 2.3.3), we noticed tiny particles darting across the video screen. These "shooting stars" appeared to be still trapped on vortices, even at temperatures less than 10 mK from transition (T_λ), presenting an opportunity to observe more vortex dynamics closer to transition than ever before. (For comparison, Paoletti *et al.* [34] tracked particles up to 50 mK near transition.) Smaller particles have the benefit that they are less affected by Stokes' drag and therefore can reside on faster moving vortices for a longer amount of time. Moreover, since the trapping force (Eq. 2.4) is proportional to the superfluid density, $\rho_s(T)$, the force is weaker near transition, meaning that only the small particles are pulled onto vortex cores near T_λ. And with less inertia, small particles are also less likely to aggregate, forming less desirable clumps. Additionally, and perhaps

most importantly, smaller particles are more passive, ensuring that the dynamics we are observe are that of the helium, not the tracer particles.

Upon further examination, we determined that these particles were likely a composition of atmospheric gas trickling into the system through an inconspicuous leak somewhere in the top of the apparatus. While we were unable to replicate these particles in precise fashion, they did provide the impetus to create extremely small particles using a drastically diluted hydrogen-helium mixture ratio. After slowly increasing the mixture ratio from 500:1 H_2:He to 50000:1, we used a mixture ratio of 10^{12}:1. We were able to illuminate and track the particles produced with this last mixture, which contained essentially a negligible amount of hydrogen. Subsequent runs used even more dilute mixtures – including just filling the mixture bottle with helium and adding no contrasting gas – and still usually produced visible, useful particles. Most likely, there is still some external source of gas (i.e. a leak) in the injection system that is contributing to our observed particles. It should be noted, however, that even if these particles were not observed with the previous camera, they still could have been present. Recent optical estimations (performed principally by colleague Enrico Fonda) calculated an average particle size on the order of 100 nm for this new approach, which suggests that we might term these tiny particles "nanoparticles." (For reference, previous experiments used a mixture ratio between 50:1 H_2:He and 500:1 H_2:He and generally produced particles on order of one to ten microns in size.)

Over time, particles tend to aggregate owing to van der Waals forces. The tiniest of particles grow slowly in size while the larger particles tend to clump. Since solid hydrogen has a density of 0.088 g/cm^3 while liquid helium's density is approximately

0.146 g/cm^3 (near T_λ) [22], larger hydrogen ice clusters float out of the testing region and up to the surface. While this mechanism is excellent for ridding the system of large particles, cooling below T_λ ($\sim$2.17 K) to testing regimes (often $\leq$2.0 K) takes several minutes, frequently leaving too few particles in the system by the time the ideal experimentation temperature has been reached. Consequently, not only did the discovery of very small particles fulfill the aforementioned small-particle benefits, but it also allowed us to successfully inject tracer particles while in the superfluid state without having them rapidly amalgamate. Every run prior to these ultra-dilute runs required an injection above T_λ because injections below transitions would result in large, unusable hydrogen ice chunks (see [33, 34]). Thus, the ability to inject into helium-II well below transition presents new opportunities to explore the uncharted dynamics of superfluid helium.

While the advantages of this new method were significant, there were also a few drawbacks. Injection above T_λ still provided some of the best distributions of tracer particles, but these injections had to be significantly longer than previous experiments owing to the drastically reduced hydrogen mass fraction in the mixture. Longer injections meant that more heat was being imparted to the fluid. This added heat was especially significant after injections in He II. Additionally, longer injections meant more mixture was being used during each injection, requiring more refills of the mixture bottle. To do so required that we stop the apparatus during the rotating experimental runs in order to refill. (Note that this dilemma could easily be rectified in the future with a larger mixture holding bottle.)

Inspired by atmospheric leak particles, we also attempted to "seed" tiny particle

nucleates by using a three-way mixture of propane (C_3H_8), hydrogen gas, and helium gas. While this last method was successful in producing small particles, it was no more effective than using an extremely dilute mixture of helium and hydrogen. Nevertheless, this seeding process may have untapped potential if more refined.

2.3.2 Laser and Optical Setup

To visualize the hydrogen (or atmospheric) tracer particles suspended throughout the liquid helium, we illuminate the interior of the test section using a 3 mW (measured value $\approx$ 2.314 mW) green laser pointer, which is clamped into a three-way translating stage at the far left edge of the experimental platform (see Fig. 2.2). The laser beam is directed through a cylindrical diverging lens and a converging biconvex lens in series. If the beam is originally propagating in the x-direction, the cylindrical lens expands the beam in the y-direction. The biconvex lens then collimates the beam in $\hat{y}$, creating a relatively uniform laser sheet $\sim$10-12 mm wide in the xy-plane. Note that the size of the cryostat windows (15 mm) sets the upper bound for the ideal sheet width, while the field of view of the camera (8.2 mm^2) determines the lower bound. If the isolation cell (see Section 2.4) is being utilized, than its window size (12 mm) limits the sheet width upper bound.

For simplicity, let us assume the laser beam has a Gaussian profile – i.e. it has Gaussian transverse electric field and intensity distributions. Then, from Gaussian optics, the beam waist is simply

$$w_0 = \left(\frac{2\lambda}{\pi}\right)\left(\frac{f}{d}\right)$$

where f is the focal length, d is the initial beam diameter, and λ is the laser wavelength. With an approximate beam diameter of 2 mm and $\lambda \approx 550$ nm, we find a laser sheet thickness of $\sim$30 microns. From this value, we can determine the Rayleigh range:

$$z_R = \frac{\pi w_0^2}{\lambda}$$

The beam radius is extended by a factor of $\sqrt{2}$ when traveling this distance. Thus, the length of the waist w_0 is essentially

$$w(z) = \sqrt{2} w_0$$

which implies that our laser sheet thickness is sufficiently uniform throughout the 49 mm sample space.

Once created, the laser sheet travels through the two cryostat windows in $\hat{x}$ and is deposited out of the second window into a beam dump. The other two windows (in $\hat{y}$) are blocked with heavy opaque black sheets to minimize any stray light from the surrounding room. The camera receives 90° scattered light through the axial window at the bottom of the cryostat.

2.3.3 Camera

The decision to switch from having the camera in the lab frame to placing it in the rotating frame necessitated purchasing a new camera. Several months of research, grant writing, and product testing thus ensued, ultimately resulting in the purchase of a state-of-the-art Princeton Instruments EMCCD camera called the ProEM, which was released in late January 2009. As mentioned in the previous sections, this new addition to the

liquid helium experiments greatly extended our ability to capture the minute vortex dynamics.

The preliminary axial-view experiments for rotating He II – that is, with the camera in the lab frame – had employed a (borrowed) Princeton Instruments PI-MAX intensified CCD (ICCD) camera. This device had a 512 $\times$ 512 field of view, 16-bit dynamic range, and a 24 μm pixel size. The new ProEM was also equipped with a 512 $\times$ 512 field of view and 16-bit dynamic range, but each pixel was only 16 μm, corresponding to an 8.2 mm $\times$ 8.2 mm image size. The pixel size was not, however, what gave the ProEM its edge: the ProEM produced images using a back-illuminated electron multiplying charge coupled device (EMCCD). For extremely low-light events where there may be only a few photons scattered off of each particle, the electron multiplying (EM) gain amplifies the weak input signal to a level well above that of the noise floor at any readout speed. This novel mechanism is especially important for acquisition at higher frame rates since there may not be sufficient time to accumulate enough photons otherwise. (Nevertheless, it is paramount that only the minimum EM gain be used to reduce long term aging effects of the CCD, as well as to prevent bright objects from saturating the chip.)

In addition to the EM gain, the ProEM features a back-illuminated (planar) sensor, which means that the photons are incident directly on the chip as opposed to having to travel through circuitry and other components in the less expensive, but less effective front-illuminated sensor. Because of this more direct path, the photons that collide with a back-illuminated device successfully produce a signal up to 95% of the time (for a certain wavelengths of light – see Fig. 2.3). More specifically, the ProEM

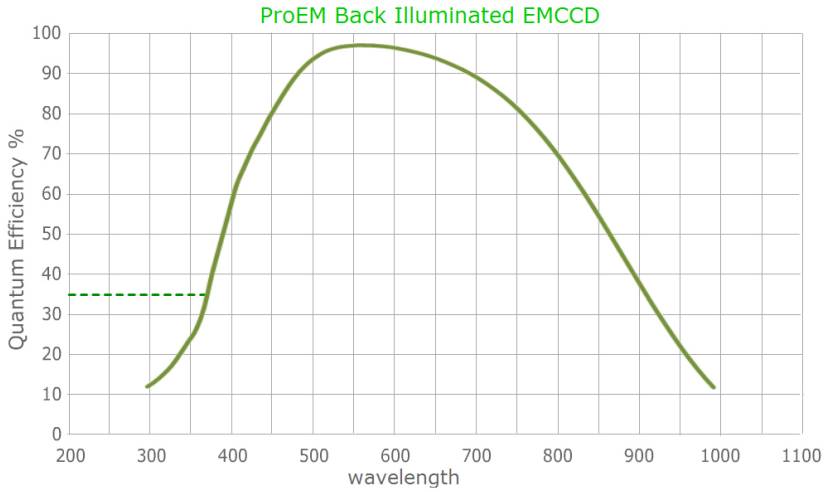

Figure 2.3: The rated quantum efficiency for the ProEM camera from Princeton Instruments. Quantum efficiency is, essentially, a measurement of a device's electrical sensitivity to light. For our green laser light, the quantum efficiency is over 90% indicating that at least 9 out of every 10 photons are successfully read by the detector and produce a signal.

offers nearly 95% quantum efficiency for green-range light like that of our laser pointer. Furthermore, the ProEM has a built-in low-noise fan that produces deep cooling to reduce thermal electric dark noise, which would further distort low-light signals. In all of the experiments performed using this camera, the EMCCD was air cooled and locked to -70°C for at least 20 minutes before the first acquisition. The ProEM also has the lowest read noise on the market (at the time of writing). The overall lower excess noise and increased sensitivity are the major factors that posit EMCCDs as decisively superior to their ICCD predecessors for our experimental purposes. It is because of these factors that we have been able to see tiny particles – at least an order of magnitude smaller than those recorded with the PI-MAX – which would have previously been undetectable.

For the majority of the data presented here, the ProEM camera was operated at 10 Hz multiplication gain in frame transfer mode. For most movies, full chip 512×512

frames were processed at $\sim$30 frames per second (fps) using the minimum exposure time, which is set by the fastest readout rate for the given frame size. The EM gain was only utilized for very low light situations. All data were transmitted to the computer on the rotating apparatus via high bandwidth Cat 5e/6 gigabyte ethernet (GigE) directly. (Note: It was necessary to switch from the more convenient mini-laptop to a full desktop PC in order to accommodate the proprietary ethernet card.) Once there, the data were acquired and processed using WinView32 and ImageJ software. A 105 mm Nikon macro lens with 1:1 magnification was attached the camera for all of the data acquisition.

2.4 Isolation Cell

In order to observe the low-energy triangular lattice array, it was crucial that our system be as isolated as possible from thermal gradients and other factors that could excite or drive turbulence throughout the fluid. Moreover, since quantized vortices must begin and end on a boundary such as the container walls or free surface, we wanted to encourage the vortices to end on a nearby surface located in the *xy*-plane, such as a lid, instead of curving radially toward the container walls or stretching to meet the free surface. (There proved to be further benefits in limiting the vortex interaction with the free surface which will be described in Chapter 3.) Our response to this criterion was to design and construct an isolation cell that would be suspended in the center of the test section.

This isolation cell was built primarily out of Delrin tubing, clear glass microscopic slides, and a smidgen of vacuum grease. Delrin was chosen for its machining ease and

Figure 2.4: Image and diagram of the isolation cell

excellent thermal stability. The outermost boundary of the cell is a black Delrin cylinder two inches high with a 1.375” inner diameter and 1.50” outer diameter (see Fig. 2.4). A 0.59” (15 mm) circular aperture has been cut out of the side in three locations, 90 degrees from one another, arranged to align with the cryostat windows. On the last side is a 0.4” slit designed to allow the laser sheet to pass through it but to block other light.

The cylinder is capped on both ends by 48 cm (diameter) black Delrin disks. The bottom disk has a one-inch square cutout with an 1/8-inch ledge, upon which a 1” $\times$ 1” microscope slide rests. A very fine layer of vacuum grease lines the ledge and corners to minimize interactions with the surrounding helium. The top disk has a central quarter-

inch hole so that tracer particles can enter the cell from the injector tube above it. Both the top and the bottom disks have a $1/8$" azimuthal groove cut into them so that they can snap securely to the main cylinder. Directly above the top disk is another identical black disk that supports the stainless steel injector tube with a wide-lipped connector rod and a set screw. The location of the end of the injector tube varied from 0.2 - 0.06 inches above the cell lid. At the edge of each disk, diametrically opposed to one another, are two 0.11" holes that direct two #4-40 threaded rods, aligning and supporting the overall cell structure.

Inside the main cylinder is a four-walled square enclosure made out of microscopic slides and white Delrin braces. (Note that white Delrin was used purely because it was only color available in that size. Black, with its lower albedo, would have been more ideal.) The braces are 90-degree corner supports that have a 0.06 inch groove cut vertically into each edge. These grooves are lined with an extremely fine layer of vacuum grease to establish a sealed edge. The braces were designed to increase the stability of the interior structure and foster an ease of assembly while still accounting for the contraction of the glass and plastic when below 4 K. Four 0.65" $\times$ 1.97" glass slides were hand-cut and slid into place between the braces. The entire unit snaps together quickly, securely, and consistently and can be transported or stored without worry of misalignment.

Chapter 3

Observations and Preliminary Analysis

As the history in Chapter 1 illustrates, superfluid helium has a way of presenting fascinating, unexpected phenomena, even when ones initial pursuits may have been directed elsewhere. In this case, we were hunting for the elusive vortex lattice array that Feynman had predicted in 1955 [35]. We found the lattice (or something close to it – see Fig. 3.1), but we also identified Tkachenko waves, surface waves, differential rotation, mixing. shearing, and evolving superfluid eddies or inertial modes. In this chapter, we catalog the observance of these phenomena and describe the circumstances under which they were discovered and subsequently studied.

All of the data and analyses presented here are preliminary. Many of the phenomena described below have never (to our knowledge) been witnessed or documented before in helium-II, so extensive follow-up research is critical. Suggestions for future research and experiments are presented in Chapter 4.

3.1 Initial Observation of the Lattice

Our first observation of the vortex lattice was captured with the camera in the lab frame. Thus, the images had to be processed and "unwrapped" before any distinct structure became apparent. Figure 3.1 shows a single frame in which the lattice formation is manifest. There is substantial structure, but also significant departure

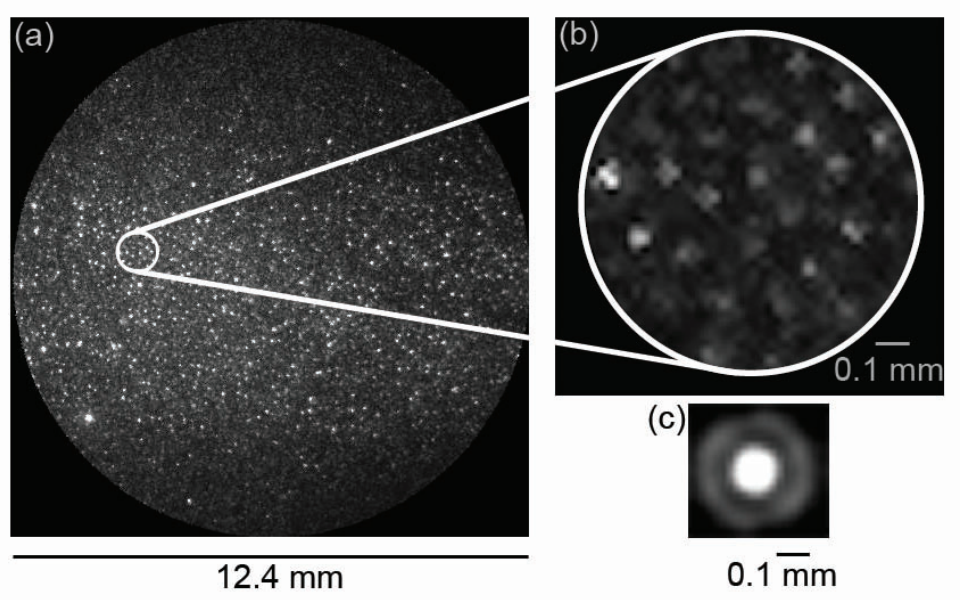

Figure 3.1: (a) One of our first observations of the vortex lattice array in helium-4. For scale, the image is 12.4 mm in diameter. (b) The zoomed image highlights a well-defined lattice structure, but deviations from the triangular array are undeniably evident. These deviations are likely a consequence of internal waves and small perturbations propagating throughout the fluid. (c) An auto-correlation of consecutive movie frames allows us to calculate the spacing between each vortex. At $\sim$5 rad/s ($\sim$0.8 Hz), Eq. 1.12 predicts lattice spacing of $\sim$0.1 mm apart, and indeed, the auto-correlation ring gives a measured vortex line spacing of 0.10 mm – a value in rather good agreement with Feynman's prediction.

from the theoretical limit of a triangular lattice. We believe that such deviations arise from boundary effects and small amplitude inertial waves called Tkachenko waves that propagate throughout the fluid. Another reason that this image shows more substantial departure from predicted values is that a single frame is a nearly instantaneous record of the lattice at that moment; there is no time averaging.

Interestingly, even when time averaging is incorporated, the lattice structure remains slightly irregular. Namely, the auto-correlation in Fig. 3.1 is more of a ring, indicating that, indeed, we do not have an ideal triangular lattice (which would produce a hexagonal auto-correlation). We believe these deviations may be a consequence of

Tkachenko waves, surface waves, and boundary effects.

3.2 Tkachenko Waves

In 1966, Tkachenko, a Russian theorist, showed that small perturbations of the vortex lattice would give rise to normal modes (plane waves). These perturbations would manifest themselves as elliptical motions of the vortices about their equilibrium positions. Moreover, he showed that only triangular lattices, or approximately triangular lattices, would allow stable oscillations. All other configurations, including quadratic, would be "absolutely unstable" [45].

In 1984, Andereck and Glaberson first observed Tkachenko waves indirectly in superfluid helium [48] using a series of thin aluminum disks. More recently, Coddington *et al*. have observed and measured Tkachenko wave frequencies in Bose-Einstein condensates (BECs) [47] (see Fig. 3.2). These waves were induced by single atom removal in a previously stable lattice array.

Now, we have achieved what we believe to be the first direct observations of Tkachenko waves in superfluid helium along the plane of propagation. The oscillations are quite evident and appear reasonably stable; however, their amplitude exceeds theoretical expectations from small-amplitude oscillations observed in BECs in Figure 3.2. In addition, our oscillations are slightly more complex and are difficult to quantify in a still image.

From Fig. 3.3, we see that there exists a strong dominant frequency, as well as a phase shift throughout the bulk of the fluid which indicates the drift of the lattice over

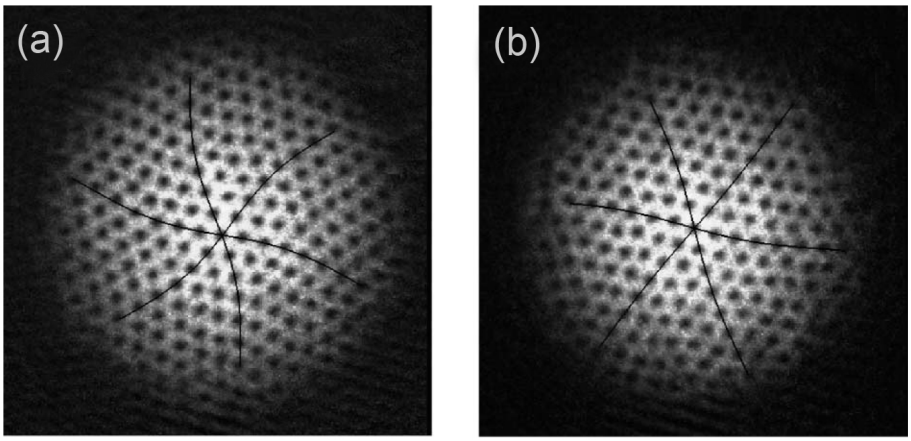

Figure 3.2: Observation of Tkachenko waves in BECs from [47]. (a) Removal of a single atom perturbs the vortex lattice causing planar wave modes to form and propagate. (b) After 1650 ms, the waves are dissipating and the triangular lattice structure is reestablishing itself. Sinusoidal lines have been fit to the wave motion throughout the lattice.

time. We can measure the fundamental frequency from the two-dimensional FFT and the energy-time uncertainty relation, $\Delta\omega\Delta T \geq \frac{1}{2}$. Solving for frequency, we have

$$\Delta\omega \quad \geq \quad \frac{n}{2\Delta T} \tag{3.1}$$

where n is the number of pixels between zero and the fundamental frequency (This pixel value could, just as simply, be considered a frequency.) and ΔT is the total elapsed time of the video. Thus, for Fig. 3.3 (which corresponds to the video online), we find $\omega = 0.75$ rad/s, which corresponds to a dimensionless frequency of $\omega/\Omega = 0.95$ or roughly equal, indicating that the frequency of the waves in the helium, ω, is roughly equal to the rotation rate of the cryostat, Ω.

In attempting to understand the motion of the waves in Fig. 3.3, we derived much of our analysis from [49] who also studied the movement of Tkachenko waves in superfluid helium.

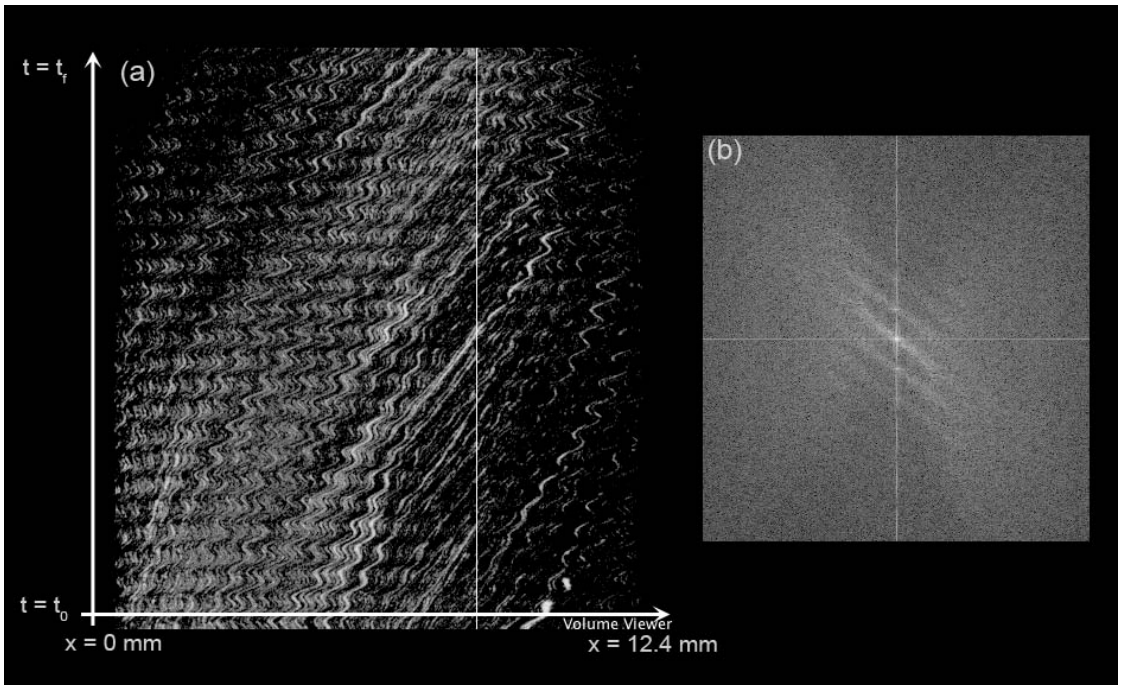

Figure 3.3: (a) Space-time plot depicting the surface waves from a rotating run (no isolation cell) and $\Omega \approx 0.79$ Hz. By virtually stacking all of the frames of a movie on top of one another, we can obtain a three-dimensional plot in time. Taking a cross-sectional slice of this 3-D plot, we find a two-dimensional space-time plot which illustrates the wave propagation. The horizontal axis gives a spatial slice of each image, measuring from 0 to 12.4 mm, while the vertical axis tracks elapsed time. (b) A 2D FFT of figure (a) plots the intensity (white peaks) as a function of frequency (vertical axis) and wavenumber (horizontal axis). Both plots were generated using the imaging software ImageJ.

Since we have a bounded system, we have discrete wavenumbers: k_z and $\mathbf{l}$, a wavevector composed of radial and azimuthal components, l_r, l_ϕ. Using the canonical definitions, Tkachenko waves are purely transverse waves ($k_z = 0$) while Kelvin waves are entirely longitudinal ($\mathbf{l}^2 = 0$). To find the dispersion relations for our system, we first consider the $l = 0$ case as the mean intervortex spacing becomes infinitesimally small ($kb \to 0$), giving a wave frequency of

$$\omega = 2\Omega_0 + \frac{\kappa k^2}{4\pi}\{\ln(1/ka) + 0.1159\} \tag{3.2}$$

for liquid height a and vessel (cryostat) rotation rate Ω_0. Eq. 3.2 suggests that we should observe a wave frequency twice that of the cryostat rotation rate; however, we saw above that these two frequencies were nearly equal. Thus, we conclude that we do not have pure Kelvin waves. Note that 0.1159 is a correction term for hollow core vortex; a liquid-filled vortex would require an additional 0.25.

In the case of $k_z = 0$, we utilize a dispersion relation of

$$\omega^2 = \frac{\Omega_0 \kappa}{8\pi} l^2$$

also from [49]. With our measured values of $\Omega_0 = 5$ rad/s and the relation $\lambda = {}^{2\pi}/_{l}$, we find $\lambda \approx 0.2$ mm; yet, the observed wavelength is 10-20 times larger than that, diminishing the likelihood of a pure Tkachenko wave.

Thus, we believe that we have a mixture of azimuthal and axial wave modes. This superposition of modes may be correlated to the presence of gravity-capillary waves from the cryostat rotation and the free surface of the fluid.

3.3 Surface Waves

Gravity-capillary waves are a type of surface wave whose dynamics are affected by both gravity and surface tension as well as fluid inertia [55]. For classical fluids, these waves grow out of the inherent restoring forces in the system – predominantly gravity for gravity waves and capillary action (surface tension) for capillary waves. In our system, it is likely that we have not only these effects, but also the influence of the vortex line length tension. That is, the surface waves we have observed are likely driven and maintained by a quantized vortex restoring force.

These surface waves were first evident by observing distinct, periodic variation in the laser light intensity during rotating runs. We soon recognized that this "blinking" was always preceded by modal oscillations of the fluid. This effect was especially apparent when performing experiments with the isolation cell because the wave modes would dominate the particle motion long before the free surface came into view; yet the two occurrences always appeared together, separated by a relatively consistent lapse of time. Thus, we conclude that the free surface is experiencing a type of gravity-capillary oscillating mode that influences the system at all times. When performing experiments with the isolation cell, these effects are minimized until the free surface is below the cell lid; however, we are unsure as to the extent of the oscillations throughout the bulk of the fluid when the cell is not present. Knowing the liquid helium level in the test section and tracking any evidence of periodic wave modes may help us to better understand that relationship.

Aside from their hallmark blinking, the surface waves can be easily characterized

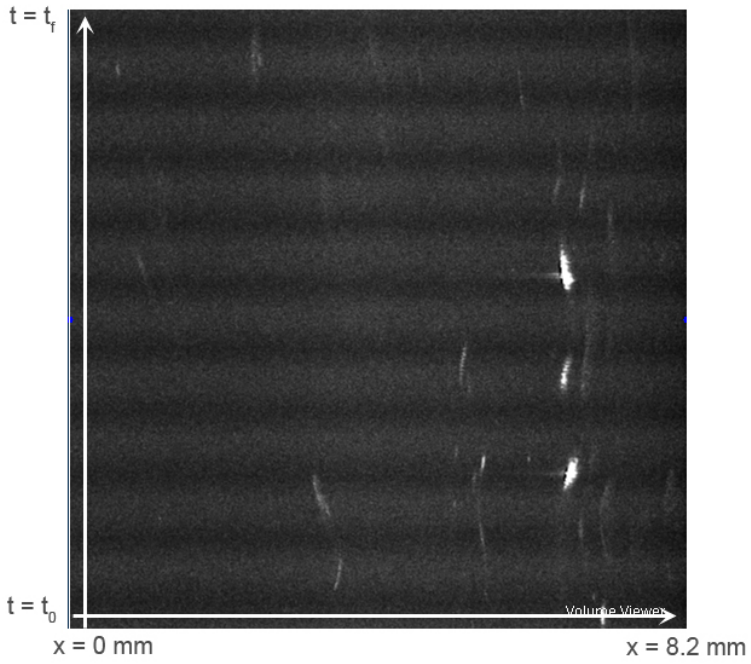

Figure 3.4: Space-time plot depicting the surface waves from a rotating run with the isolation cell and $\Omega \approx 0.315$ Hz. The image was created by stacking all of the video frames in time and then taking a 2-D slice. The horizontal axis depicts the field of view of the camera from 0 - 8.2 mm while the vertical axis tracks the elapsed time of the video ($\sim$47 s in this case). The horizontal stripes are signatures of the surface waves which result in periodic oscillations of the laser light. The vertical waves are tracks of particles that oscillate with a similar, but not identical, frequency.

by viewing a "volume" of video images (see Fig. 3.4). When the individual frames from a video are stacked in time, the variations in laser light are immediately evident in periodic horizontal stripes. An FFT of Fig. 3.4 allows us to calculate the frequency of the surface wave, and we find $f_s = 0.107$ Hz, or a dimensionless frequency $f_s/\Omega = 0.34$. Note that this value is approximately a third of the dimensionless frequency of the Tkachenko wave modes, indicating that they are two distinct phenomena, although their actions may still be systematically coupled.

3.4 Differential Rotation

After inserting the isolation cell in the system, we observed a phenomenon never before witnessed (to our knowledge) in helium-II – differential rotation. Differential rotation occurs when the angular velocity of a non-solid spinning body varies with radius. It is commonly found in accretion disks, galaxies, protostars, the sun, and the atmospheres of Jovian planets like Jupiter and Saturn where the gas near the equatorial region rotates faster than gas near the poles. In galaxies, the shorter orbits of the stars near the center result in the stellar spiral arms adorning galaxies across the universe several millions of years later. In stars, the inner differential rotation plays a crucial convective role, transporting heat throughout the stellar core as well as mixing various elements to aid in its evolution. In neutron stars, the intricate workings of the inner core are of special interest owing to their possible superfluid composition, which may be responsible for observed phenomena such as pulsar glitches [56].

In our system, we observe a unique, statistically steady subrotating cylinder at the center of the isolation cell. It rotates differentially with respect to the outer radii, which either co-rotate or slowly superrotate. This specific differential form occurs when we inject above T_λ, slowly cool the system through transition and begin rotating the apparatus (at any rate). During the first moments of spin up, there is no differential motion: the fluid appears to spinning up together, obeying general Newtonian flow properties. But within a few minutes, the outer regions begin stabilizing (co-rotating) while the center subrotates within a distinct radius, possibly forming a shear layer or Stewartson layer (see Fig. 3.5).

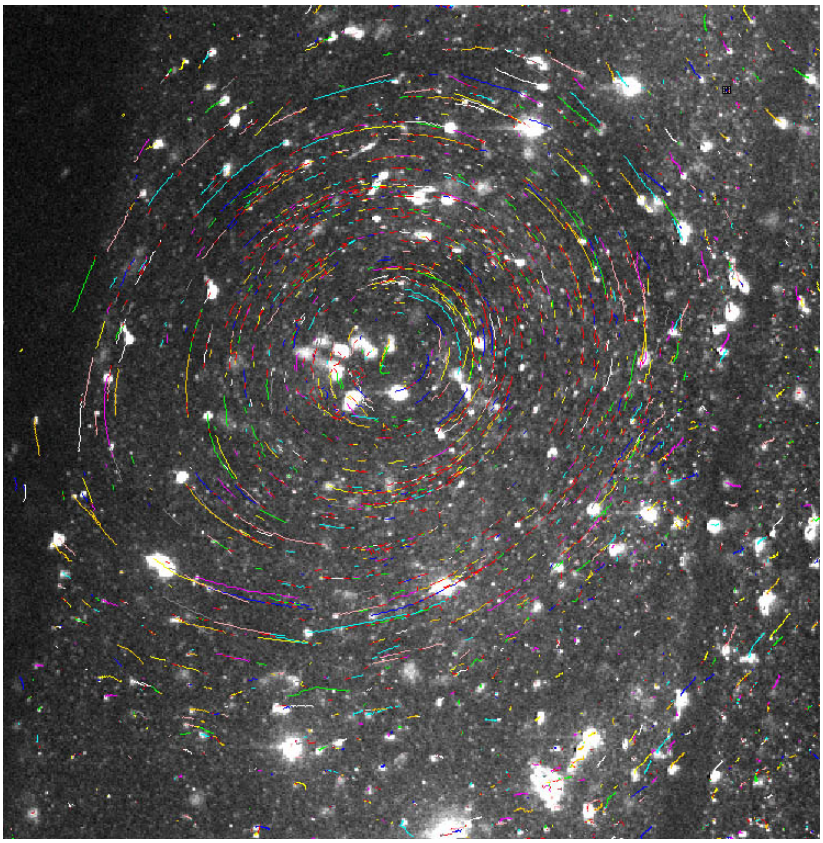

Figure 3.5: Individual particle trajectories from 2.7 seconds of a real-time video analyzed using ImageJ particle tracking software [59]. Each track represents a single particle trajectory without regard to angular velocity, although differential subrotation is apparent in the center of the image and in the full video. Note the well-defined Stewartson boundary layer. The particles near the edges of the frame are either co-rotating (few visible tracks) or slightly superrotating (short tracks near lower right-hand corner).

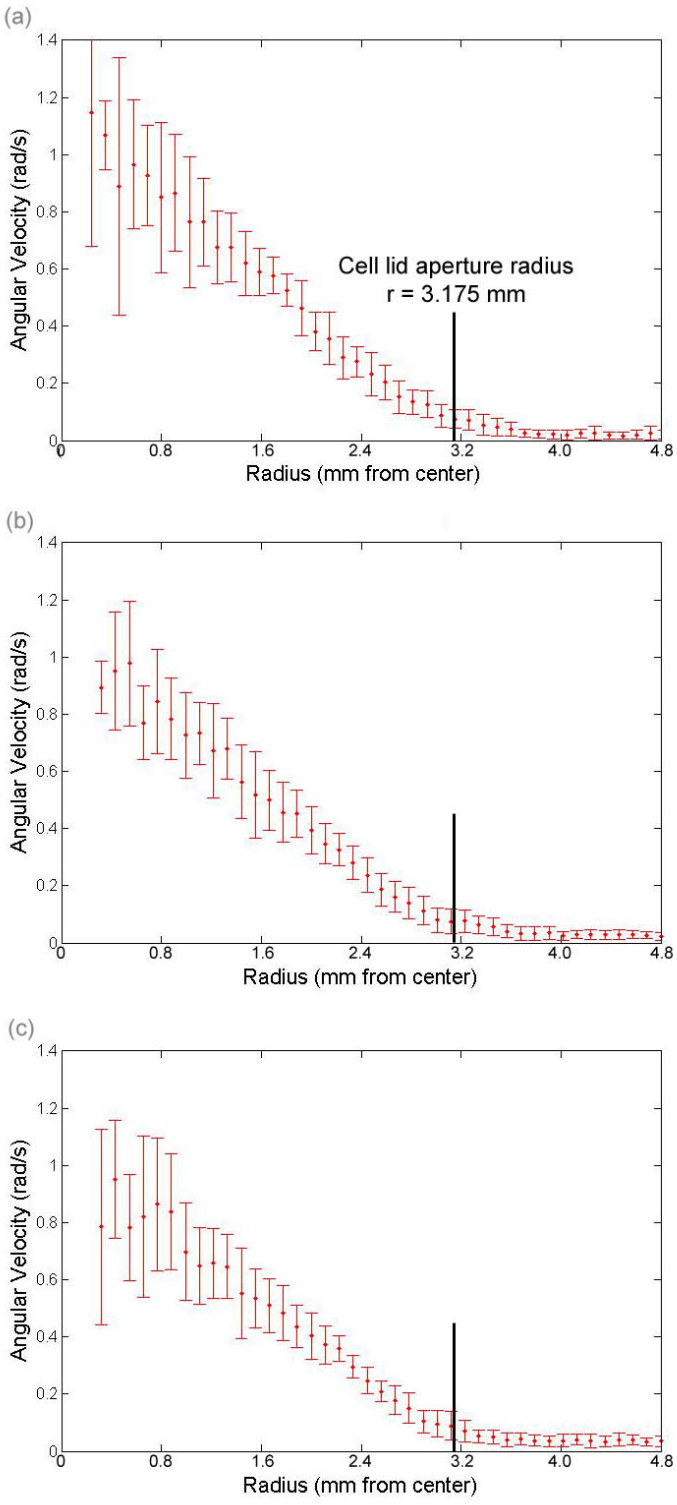

Figure 3.6: Plot of the mean angular velocity of each particle as a function of radius for three consecutive time segments (a)-(c), generated using particle trajectories seen in Fig. 3.5. The average angular velocity of the differential rotating particles tends to decrease in time, while the particles located at $r \gtrsim 3.2$ mm from the center appear to be nearly co-rotating.

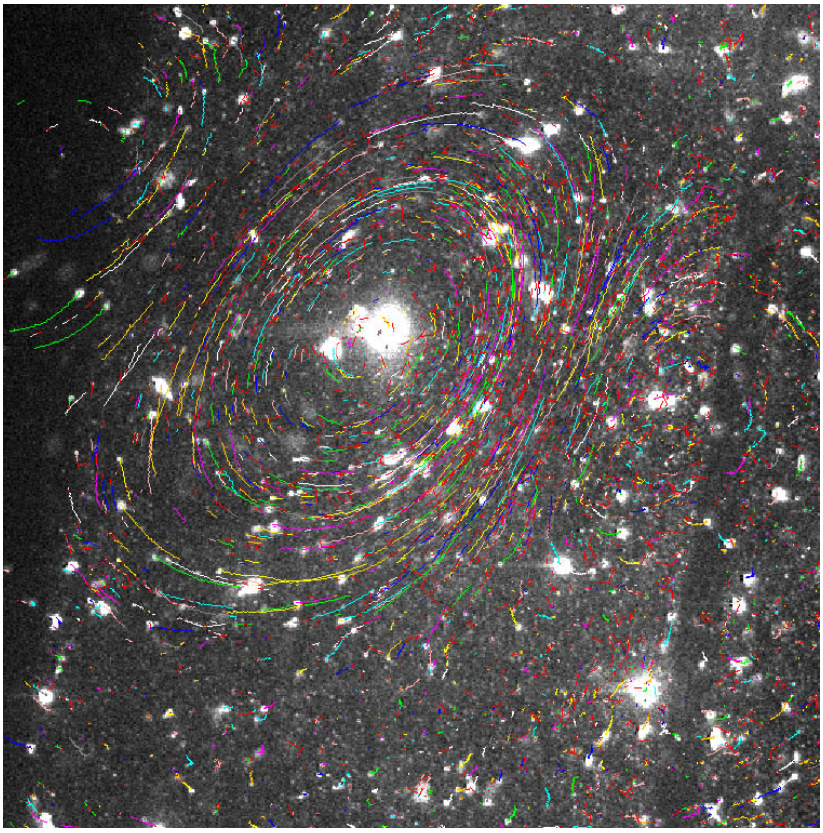

Figure 3.7: Particle trajectories depicting the evolving eccentricity of the cylinder, induced by instabilities in the system. The eccentricity of the elliptical structure remains dynamic as turbulence propagates.

In fact, the differentially rotating cylinder is only quasi-stable as, after a few minutes of defined structure, the cylinder begins shearing or mixing with the co-rotating fluid. This development is most likely a consequence of a Kelvin-Helmholtz instability whereby a velocity or density difference between two shearing media induces turbulence in a fluid. The mixing we observe is often elliptical, indicative of the lowest energy, or $m = 2$, Kelvin-Helmholtz mode. (The K-H mode for $m = 1$ is stable.)

The mechanism causing the differential in first place is less readily identifiable. Here, we present a few possible explanations for the motion we see, but further experimentation and review is necessary. First and foremost, the effect of the quantized

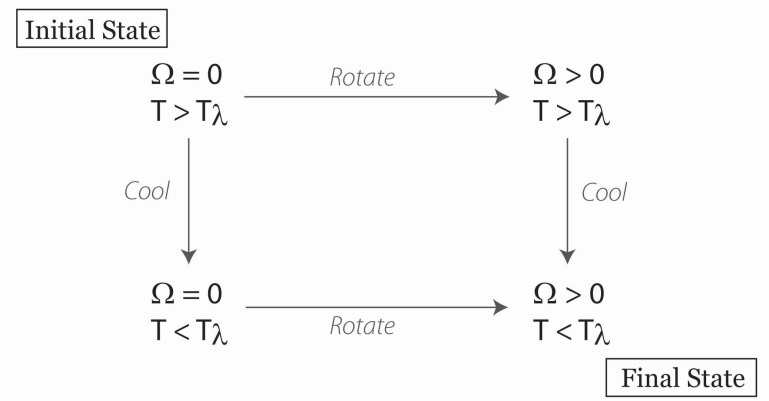

Figure 3.8: Commutation diagram outlining the possible paths to reach a steady-state equilibrium while cooling. It suggests that the order of system rotation versus cooling may affect the dynamics of lattice formation. The analysis presented in Fig. 3.6 is an example of the counterclockwise path: Injection above transition, cooling below T_λ, and then rotation.

vortices in these flows is unclear. Since the vortices must terminate on some boundary, it is possible that the vortex lines in the center of the isolation cell are travelling up through the cell lid aperture and are terminating on the injection tube walls directly above it. They might also curve out of the cell lid towards the cryostat walls, which could drive instabilities (or at least perturbations) in the lattice. Additionally, the central vortices could simply pin themselves to the edge of the lid aperture.

In all of these cases, the system was being evaporatively cooled and thus, there was some need for heat flow throughout the cell. After sealing all of the cell windows with a fine layer of vacuum grease[1], the design of the cell only left two main avenues for the dissipation of the thermal energy that is rapidly imparted to the system with every injection – the small space between the cell lid and the window enclosure, and the 1/4" hole in the center of the lid. It is possible, then, that the differential rotation is actually a

[1]Initial test runs showed that the small crevices between the windows and their supports – originally designed to allow liquid helium to fill the cell but to otherwise keep it very isolated – actually resulted in more turbulent motion throughout the cell. As a result, the crevices were sealed with vacuum grease and the cell lid was loosened slightly.

sort of heat transport process whereby heat is cycling through the hole, around the shear layer, and back out to the liquid helium bath surrounding the cell.

Several points support this theory:

- If the differential rotation reaches a steady (or quasi-steady) state, it does so in the center of the cell (directly beneath the hole) with a similar radius every time, regardless of the apparatus rotation rate.
- The differential structure ends abruptly when the liquid helium temperature is stabilized.
- The strong differential cylinder and/or Stewartson layer was not evident in any of the runs without the isolation cell.
- The captured images of the system bear a striking resemblance to images of classical convection in a rotating cylinder (see Figure 3.9 on page 50).

Yet, there is no reason to believe that the convective process is natural to a superfluid. Indeed, as [54] have shown in counterflow experiments, heat is transported ballistically via the normal fluid and does not convect classically. (The superfluid, with zero entropy, cannot transport heat at all.) Even so, it is possible that geometry of the cell and the mutual friction between the vortices and the normal fluid is driving some unique convective motion.

On the other hand, by analysis of the specific angular momentum of the system, one can postulate that cooling causes differential rotation. Consider that as the liquid helium cools below T_λ, the relative density of the normal fluid to the superfluid decreases,

Figure 3.9: Classical convection in a rotating cylinder by [53]. In this image, the vessel is heated at the rim and cooled at the center, driving convection.

i.e. $\rho_n \to \rho_s$. Then the total angular momentum of the system can be written as

$$L_z/h = \rho_s l_{zs} + \rho_n l_{zn} \tag{3.3}$$

where h is Planck's constant and l_z is the specific angular momentum:

$$l_z = \frac{L_z}{\rho h} \tag{3.4}$$

Moreover, since the quantized vortices in the superfluid carry more angular momentum than the normal fluid component, we find that $l_{zs} > l_{zn}$. It follows that $\frac{dl_{zn}}{dt} > 0$ as $\frac{d\rho_n}{dt} < 0$, suggesting that cooling causes differential rotation. Likewise, this argument suggests that heating would induce differential rotation in the opposite direction; however, this result was not observed in our experiment and should be investigated further.

It is also important to note that many of the runs with differentially rotating centers

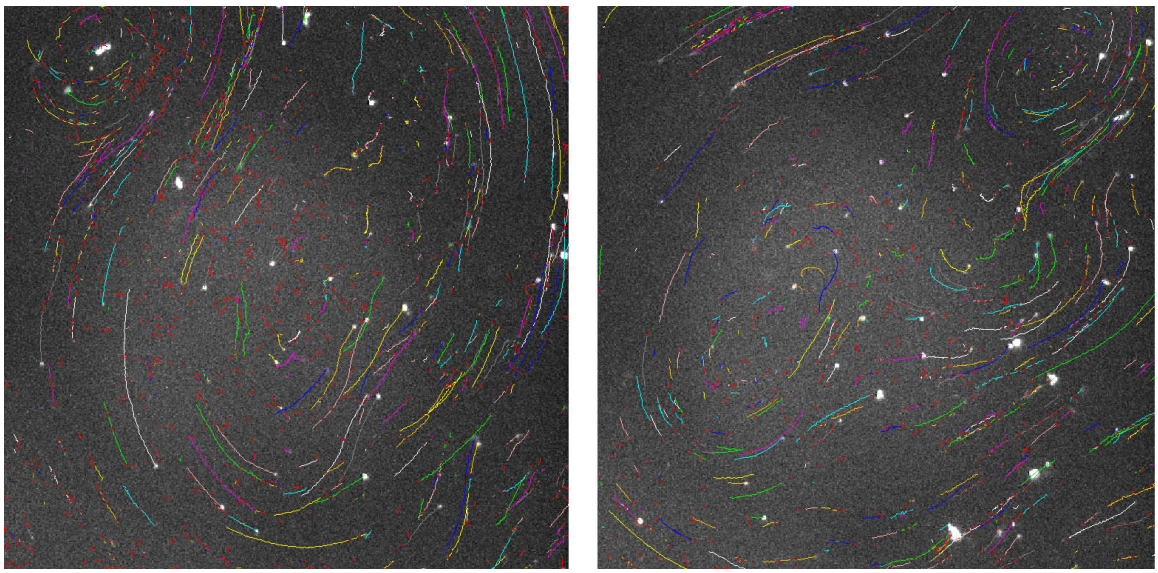

Figure 3.10: Evidence of eddy generation and propagation throughout helium-II, analyzed using ImageJ particle tracking software for two 3.3-second segments of video. (left) The first eddy, seen here in the upper left-hand corner of the image, appeared $\sim$30 seconds after rapidly cooling below T_λ while rotating at .35 Hz. (right) The next eddy, seen here in the upper right-hand corner of the image, formed independently $\sim$10 seconds later.

possessed well-structured outer edges or radii – possibly a co-rotating lattice, though almost certainly not the lowest energy triangular array. The turbulent motion from the center seemed to distort any uniform spacing or precision arrangement near the edges, but this occurrence should be studied further.

We also observed other forms of poorly understood turbulent phenomena in helium-II. For example, when perturbing the system (e.g. via global temperature modification), we would occasionally observe the generation and propagation of rapidly rotating vortex bundles, or "superfluid eddies" (see Fig. 3.10). These tightly wound bundles would spontaneously generate and dissipate on timescales comparable to the system rotational period. Additionally, we observed situations whereby the central fluid would undergo vortex reconnection while the remaining fluid underwent uniform spin-up. While we

know that vortex reconnection is a mechanism for energetic minimization, the extent of its role in rotating helium-II is unclear.

Chapter 4

Conclusions and Future Work

We have successfully designed and built a rotating experiment that has initiated a new study of the lattice structure and dynamics of quantized vortices in superfluid helium with unprecedented depth. The setup employs marked improvements over its predecessors, including control of the entire apparatus from the rotating frame, installation of a new EMCCD camera which allows for imaging nanoscale tracking particles, and the development and implementation of a new isolation cell which permits investigation into new phenomena such as differential rotation in helium-II.

Furthermore, we have developed new techniques of tracer imaging based on tiny particles, orders of magnitude smaller than those previously visualized. This discovery promises immense improvement in the ability to observe the vortex dynamics in helium, ensuring that the tracer particles remain passive as well as enhancing the capabilities of imaging quantized vortices very near the λ-transition. It also presents the novel capacity to inject below T_λ – directly into the superfluid-dominated domain of helium-II – promoting further study of this exotic and relatively unexplored regime.

After only a few months of data acquisition, our new apparatus has already provided a wealth of novel observations and unexplained phenomena while testing the scope of current theories. We have observed the vortex lattice dynamics in the (r, ϕ) plane (i.e. along axis of rotation or longitudinal to the vortices) and have presented the

first ever visualization of Tkachenko waves in helium-II from this view. Additionally, we have seen evidence of differential rotation with distinct Stewartson layer boundaries, Kelvin-Helmholtz instabilities, and the formation and propagation of superfluid eddies. We have also documented the presence of gravity-capillary surface waves that conclusively demonstrate an interaction between the liquid helium free surface and the bulk of the fluid. Even so, these observations are only a small sample of the new regimes that our experiment can explore, and our main contribution is likely the experiments that we have made possible, rather than those which we have already performed.

4.1 Future Research

Time is frequently the limiting factor in experimental science, and this project was no exception. But what is inconclusive to one is fodder for the next aspiring scientist. Thus, the following list contains several suggestions for future work which may yield fruitful (or at least interesting) results. Note that this list is motivated by tasks of potential scientific merit; there are several other, more mundane tasks that must be completed (such as fixing the corrupted cryostat vacuum jacket) before one may be able to embark on such explorations.

1. Calculate the angular velocity of the differential rotation as a function of cryostat rotation rate and temperature slew rate.
2. Calculate the angular momentum transfer between the normal fluid and superfluid components.
3. Determine the relationship (if any) between the size and location of the cell lid

aperture and differential rotation radius. Cell lid blanks have already been created, so this experiment would only entail drilling various diameter holes (in perhaps several locations with different geometries) and testing them systematically for all rotation rates. Additionally, the injection tube location can be easily adjusted by repositioning the nuts on the #4/40 threaded support rods.

4. Run the same experiments without the cell and specifically try to induce differential rotation (e.g. through localized thermal gradients or various perturbations).
5. Plot observed lattice spacing as a function of frequency. (Will need to perform more experiments with current setup.) Verify this spacing by adjusting the laser position.
6. Obtain more comprehensive observations and measurements of the system heating, whether directly with a heater or indirectly by the cessation or reduction of evaporative cooling. The latter requires experimental finesse and advanced system temperature control sensitivity (e.g. by reconfiguring the current pneumatic valve PID settings)
7. Run the aforementioned experiments with larger (i.e. $d \geq 1$ μm) particles, especially when testing for the lattice. Established theory (see [33]) mandates that particles that are too large can alter the dynamics of the system and artificially stabilize vortices; however, personal empirical evidence suggests that particles that are too small may hinder a readily quantifiable lattice structure. Determine if larger particles aid in lattice stabilization.
8. Calculate the energy difference between a triangular lattice array and a quadratic array, as well as the energy necessary for higher order arrays.

9. Calculate the vortex line length tension or restoring force for the observed gravity-capillary waves.
10. Further the frequency and phase analysis of Tkachenko waves and surface modes.
11. Determine the source of the volunteer "leak particles" from Section 2.3.1, and develop a controlled injection mechanism.
12. Fix, purchase, or manufacture a liquid helium level sensor for the test section in order to quantify the influence of the free surface on the observed phenomena.
13. Purchase or manufacture a temperature sensor for the liquid helium reservoir. This addition would allow one to determine the thermal influx during refills of the test section.
14. Compare the rotation effects in helium-II to that in helium-I (or even in another classical substance like liquid nitrogen or water). More specifically, consider the heat transport mechanisms and the effects of the cell geometry to that in a classical fluid.
15. Develop or determine fluid equations of motion that could describe the classical phenomena (e.g. differential rotation, Kelvin-Helmholtz instabilities, eddies, convection) that we are mimicking in a quantum fluid.
16. Research the relationship between the phenomena observed in Bose-Einstein condensates, such as Tkachenko waves, and our observations in helium-II.
17. Construct a spherically symmetric cell and study spherical Couette flow in helium-II. This experiment would be especially significant to those who study superfluid cores of neutron stars. A preliminary experiment (owing to its simpler geometry) might be to study Taylor-Couette flow in helium-II.

18. Explore possible connection between Tkachenko waves in superfluid helium and inertial modes or waves in large-body rotation. Specifically probe the connections between differential rotation, vortex reconnection, and inertial waves to pulsars and inner cores of neutron stars.

Appendix A

Standard Operating Procedures (January 2010)

When I first arrived in the lab and started running, I had a hard time keeping track of every button, knob, and switch which resulted in many failed runs and wasted days (or at least, quintessential "learning experience" days). In an effort to assist myself and future helium experimentalists in the Lathrop Lab, I have compiled a few lists of standard operating procedures for various aspects of the experiment. Do keep in mind, of course, that equipment and computer programs change with time and people, and so must the details of these procedures continue to be updated. Nevertheless, the overall process will likely remain the same.

A.1 General Procedure for Helium Runs

The following abbreviations will be utilized:

VJ = vacuum jacket (listed as OVC in Oxford manuals)

cryo = cryostat

turbo = turbo molecular pump

pneumo = pneumatic

ITC = Intelligent Temperature Control – Oxford Instruments temperature control unit, utilized here for cryostat test section

ILM = Intelligent Level Meter – Oxford Instruments liquid helium level sensor

t.t. = transfer tubes

2-3 Days Before Running

1. Pump down on vacuum jacket.

   If the cryostat vacuum jacket (VJ) is at 1 atm (i.e. it has recently been opened to atmosphere for repairs), then

   (a) Open all valves from the cryostat to the roughing pump (tall vacuum jacket needle valve on cryostat, valve to turbo pump). The cryostat and all lines should be at 1 atm.

   (b) Turn on roughing pump. Wait until pressure is < 100 mTorr.

   (c) Turn on turbo pump. (Press right-most button on the Pfeiffer Balzers TCP121.)

   (d) Let the system pump down until the VJ pressures is < 1.0 mTorr.

   If the cryostat vacuum jacket is under partial vacuum (i.e. it has not been opened to atmosphere since the last experiment), then

   (a) Turn on roughing pump (keep all other access valves closed). Wait a few minutes until pressure is < 100 mTorr.

   (b) Open valve to turbo pump. Check that pressure remains < 100 mTorr and then turn on turbo pump (Press right-most button on the Pfeiffer Balzers TCP121). Wait until pressure is 2-4 mTorr. (20-40 min.)

   (c) Slowly open vacuum jacket needle valve (tall one).

   (d) Let the system pump down until the VJ pressures is < 1.0 mTorr.

2. Check that there is sufficient liquid nitrogen. Order more from GTS via Nancy

Boone if necessary.

3. Check that there is sufficient liquid helium. Order more from GTS via Nancy Boone if necessary. (Schedule it to arrive the day before or the first day of running.)
4. Realign laser optics if necessary. (It is good practice to check the laser alignment often to ensure the setup has not been bumped or otherwise compromised)
5. Backup any lonely data. (All data should have a twin!)

1 Day Before Running

System Status:

- Vacuum jacket at 10^{-4} or below (Electronic Pirani gauge should read 0.0×10^{-3})
- VJ roughing and turbo pumps still pumping on vacuum jacket
- Bath and test sections still at atmosphere filled with lab air
- Test temperature $\sim$290 K (near room temperature)

Setup

1. Plug in Oxford temperature sensor (ITC) (black cord to top of cryostat labeled "SENSOR")
2. Turn on ITC temperature sensor
3. Plug in 24V DC power supply for silver electronics box
4. Turn on Dell computer
   (a) Open *Helium_Temps_and_Logs* (on Desktop) > Create new folder with today's date (mmddyy)

(b) Open Labview VI's > New.vi

(c) **Make sure pneumatic valve button is set to *Closed*****

(d) Toggle switch at bottom to *Buttons* control

(e) Press arrow button at top of screen to begin recording

(f) Check that date on screen changes appropriately

(g) Connect to internet, authenticate network

(h) Open Matlab

(i) Run *exper*

Prepare for Fill & Flush

1. Check all valves are closed, including pneumatic valve (Bottom-most Labview button switched to *Closed*, pneumatic gauge should read $\sim$15 psi).
2. Check that input port seal is tight
3. Turn on (plug in) pneumatic valve roughing pump (sitting on metal pedestal).
   (a) NOTE: Do not plug this roughing pump into a surge protector. It draws too many amps. Plug it into one of the large grounded silver outlets.
4. Turn on He gas
   (a) Always in this order: main, gauge, regulator (left, right, middle)
   (b) Open to $\sim$3* psi (*Currently, the "zero" level on the gauge is $\sim$7 psi, so net 3 psi is $\sim$10-12 psi on the gauge)
5. Open He copper tubing gas lines (2 knobs).
6. Open both bath and test section valves (3 knobs)

Fill & Flush

1. Toggle bottom-most button on Labview to close pneumo valve (already done for first time)
2. Press 'He' on Matlab "Flushing" panel to stream helium gas through bath and test sections
3. Fill until copper nozzle emits a small amount of helium gas
4. Toggle button on Labview to open pneumo valve
5. Unpress 'He' on Matlab (Should be done just after the pneumo valve opens – $\sim$30 psi – or pedestal roughing pump will grumble loudly when it sucks up excess helium)
6. Wait a few minutes
   (a) Track pressure using grey pressure gauge
7. Repeat 3-5 times or until pressure is consistently < 10 mTorr (usually 2-4 mTorr)
8. Last Time — Leave pneumo valve closed; Leave cryo valves open with helium gas streaming through them
   (a) Turn off pedestal roughing pump (unplug)

Fill With Nitrogen

System status:

- All cryo valves open
- Pneumo valve closed
- He copper gas lines still open.

1. Attach large copper tubing insulated with black rubber (henceforth called "black

hose") to output of nitrogen Dewar

   (a) May need extra copper flange connector piece to attach to Dewar

   (b) Tighten with wrench if necessary.

2. Insert aluminum L-tube into bath section via input port (He gas should be flowing out)

   (a) Re-tighten input port seal after insertion

3. Attach other end of black hose to L-tube. Tighten well.

4. Close all cryo valves

5. Unpress 'He' on Matlab to strop streaming helium gas

6. Turn blue knob on nitrogen Dewar to inject nitrogen into bath section

   (a) Continue until liquid N comes out b.o.w. nozzle (takes ~10 min)

   In the meantime,

   (b) Turn off He gas (regulator, gauge, main – middle, right, left)

   (c) Close He copper gas lines

7. Leave black hose attached until morning

8. Leave VJ pumps running (ensure vacuum jacket valve is open)

9. Follow End of Day Procedures

   (a) Turn off computers, temperature sensor (unless tracking overnight), gauges, etc.

   (b) Unplug 24V DC power supply for silver electronics box

   (c) Make sure gas bottles are closed

Day of Run

System status (1st day of running):

- Vacuum jacket at 10^{-4} mTorr or below (Electronic Pirani gauge should read 0.0×10^{-3})
- VJ roughing and turbo pumps still pumping on vacuum jacket
- Bath section filled with liquid nitrogen
- Bath temp = $\sim$77 K (boiling point of nitrogen)
- Test temp = $\sim$280 K (read from ITC)
- Test temperature $\sim$290 K (near room temperature)

System status (Subsequent, consecutive days of running):

- Vacuum jacket off (See Notes regarding Corrupted Vacuum Jacket for alternative comments)
- VJ roughing and turbo pumps off
- Bath and test sections filled with remnant He gas, boiled off from previous day's run
- Bath temp = unknown (No bath section thermometer at time of printing)
- Test temp = 140* K (read from ITC) (*For a good vacuum jacket. Again, see Notes regarding Corrupted Vacuum Jacket for comments)

Setup

1. Ensure temperature sensor (ITC) cord is plugged into top of cryostat
2. Turn on ITC temperature sensor
3. Plug in 24V DC power supply for silver electronics box
4. Turn on Dell computer

(a) Open *Helium_Temps_and_Logs* (on Desktop) > Create new folder with today's date (mmddyy)

(b) Open Labview VI's > New.vi

(c) **Make sure pneumatic valve button is set to *Closed*****

(d) Toggle switch at bottom to *Buttons* control

(e) Press arrow button at top of screen to begin recording

(f) Check that date on screen changes appropriately

(g) Connect to internet, authenticate network

(h) Open Matlab

(i) Run *exper*

5. Turn on He gas to $\sim$3* psi

   (a) Order of knobs: main, gauge, regulator (left, right, middle)

   (b) *NOTE: Currently, the "zero" level on the gauge is $\sim$7 psi, so net 3 psi is $\sim$10-12 psi on the gauge

6. Open He copper tubing gas lines (2 knobs)

Cool Test Section with Liquid Nitrogen (Only if liquid nitrogen is in the system, of course!)**

1. Open all three bath and test section valves to allow nitrogen to fill test section (Bath valve must be open to relieve excess gas pressure from the system)
2. Monitor system until test section temperature reaches $\sim$90 K (read from ITC or Dell computer)
3. Close small capillary valve when T=90 K (closes bridge between bath and test sections)

(a) NOTE: It is vital that the system not go below (or even particularly close to) 77 K, the freezing point of liquid nitrogen

4. Press '*He*' on Matlab panel to stream helium gas into only test section (since capillary is closed)
   (a) Continue streaming until test valve pops up, indicating 2 psi in test section
5. Disconnect black hose from L-tube
6. Push L-tube all the way down into cryostat until it hits the bottom
7. *Put on safety glasses*
8. Reopen capillary valve to blow off remaining nitrogen
   (a) Direct air out of L-tube by holding finger over brass nozzle
   (b) Test section should be completely empty of nitrogen when finished
9. *Put on (or hold) welding gloves*
10. Loosen input port o-ring seal
11. Heat L-tube (if necessary) and remove
12. Place cap back on input port and tighten seal
13. Heat (if necessary) and close all valves
14. Unpress 'He' to stop steaming helium gas

Prepare for Fill & Flush

1. Check all valves are closed, including pneumatic valve (Bottom-most Labview button switched to *Closed*, pneumatic gauge should read $\sim$15 psi).
2. Check that input port seal is tight
3. Turn on (plug in) pneumatic valve roughing pump (sitting on metal pedestal).

   (a) NOTE: Do not plug this roughing pump into a surge protector. It draws too many amps. Plug it into one of the large grounded silver outlets.
   (b) Leave VJ roughing and turbo pumps on and VJ valve open
4. He gas should still be on but solenoid should be closed (i.e. Matlab button unpressed)
5. Open both bath and test section valves (3 knobs)
6. Check that helium copper tubing gas lines (2 knobs) are open

Fill & Flush

1. Toggle bottom-most button on Labview to close pneumo valve (already done for first time)
2. Press 'He' on Matlab "Flushing" panel to stream helium gas through bath and test sections
3. Fill until brass nozzle emits a small amount of helium gas
4. Toggle button on Labview to open pneumo valve
5. Unpress 'He' on Matlab (Should be done just after the pneumo valve opens (gauge $\sim$30 psi) or pedestal roughing pump will grumble loudly as it sucks up excess helium)
6. Wait a few minutes
   (a) Track pressure using grey pressure gauge
   (b) NOTE: The initial pump-down pressure will be higher when the system has recently been filled with nitrogen.
7. Repeat 3-5 times or until pressure is consistently < 10 mTorr (usually 2-4 mTorr)

8. Last Time:
    (a) Leave pneumo valve closed
    (b) Turn off pedestal roughing pump (unplug)
    (c) Close all cryo valves (3 knobs) and copper tubing gas lines (2 knobs) (He gas will still be able to flow through flexible plastic tubing)
    (d) Unpress 'He'

NOTE: The temperature in the test section will continue to rise until liquid helium begins to fill it, so time is of the essence for the next few parts. In fact, it is wise to set up for liquid helium filling (next part) while filling and flushing (previous part).

Set up for Liquid Helium Filling

1. Position helium Dewar on forklift and secure with ratchet rope
2. Teflon tape Dewar gas input nozzle
3. Open clear, flexible plastic tubing helium gas line (black knob found near pneumatic valve/pedestal roughing pump) slightly ($1/8^{th}$ to $1/4^{th}$ of a turn is usually sufficient.)
4. Fully attach flexible tubing to helium Dewar via large copper nozzle
5. Slightly close pressure release valve on helium Dewar
6. Slide brass nozzle to end of long leg of liquid helium transfer tube (t.t.)
7. Ensure helium level sensor (ILM) probe is attached to top of cryostat
8. Turn on Level Sensor (ILM)
    (a) Set rate to 'Fast' while filling (Press 'Rate' button to change)

Liquid Helium Filling

1. Climb ladder and hang short leg of t.t. from ceiling (or otherwise secure it above the cryostat)
2. Insert long leg of t.t. into Dewar (Must open top Dewar lever to do so)
3. Pressurize helium Dewar by opening and closing the helium gas input lever
   (a) Should hear helium gas streaming through the Dewar as it pressurizes the liquid inside
   (b) Should soon feel or see gaseous helium flowing out of the short leg of the t.t.
4. While regularly pressurizing the Dewar to maintain a constant flow of helium gas out of the t.t., slowly lower the long leg into the Dewar in $\sim$6-inch increments.
5. As soon as the gas flowing out of the short leg becomes cold, loosen the input port seal and insert the short leg all the way into the bath section, stopping 1-2 cm from the bottom of the bath reservoir.
6. Re-tighten the input port seal
7. Open bath section valve (sideways knob) so excess gas can flow out of brass nozzle
8. Open test section and capillary valves so helium can flow into and cool test section
9. Adjust flexible tubing knob and/or pressure release lever on Dewar so that helium gas steadily streams out of brass nozzle
10. Continue pressurizing Dewar ("open-close" gas input lever) so that gaseous stream out of brass nozzle remains strong and steady
11. Lower transfer tubes in $\sim$6-inch increments every so often to fill and cool system

slowly

(a) Try to keep t.t. connecting hose parallel to the floor

(b) Will eventually need to raise Dewar using forklift

12. As soon as the first drop of liquid helium registers on the ILM

(a) Close vacuum jacket valve

(b) Turn off turbo pump

(c) Turn off VJ roughing pump after 10-20 minutes (allow turbo to spin down)

(d) Close turbo pump valve

13. Track test section temperature and liquid level for reference

(a) Test section temperature should begin steadily falling once liquid is in the system

(b) If system is cooling too quickly (lots of ice on transfer line) or too slowly (no visible or audible stream of helium gas coming out of brass nozzle), adjust the Dewar pressure release level or the flexible tubing knob accordingly.

(c) As T$\rightarrow$40 K, the specific heat drops dramatically and the temperature will begin fall much more rapidly

14. Re-pressurize Dewar whenever ILM level begins to fall

(a) Continuing pressurizing the Dewar until T$\approx$4.2 K (Should see relative flat-line on temperature graph)

(b) Eventually, ILM should reach 101.1%, indicating the bath section is full of liquid helium

(c) Check that liquid helium is visible in test section (Should see boiling/bubbles)

(d) Once the above stipulations are met, make sure that the level does not fall

substantially (or at all) between ILM "fast rate" readings. Any gross fluctuations in level indicate a strong thermal gradient, which should be avoided. Continue filling with helium until ILM = 101.1 consistently.

15. Heat valves and input port
16. *Put on welding gloves!*
17. Close all valves on cryo and open pressure release valve on Dewar
18. Loosen input port seal
19. Remove transfer tubes
    (a) Cryo first
    (b) Dewar second
    (c) May need assistance to lower forklift while removing long leg from Dewar
20. Replace input port cap and tighten seal
21. Close top valve/lever on Dewar
22. Change ILM rate to 'Slow'
23. Close flexible tubing knob and turn off helium gas

Cooling the System from 4.2 K to 2.25 K

Note: Process normally takes about an hour.

1. Turn on (plug in) pneumatic valve/ pedestal roughing pump (if not on already)
2. Set Labview 'Temp Set Value'= 2.2
3. Set 'upper limit'= 1.200
4. Clear chart (right-click on Labview graph) if desired.
5. Open test and bath valves (but not capillary)

6. Increase ‘upper limit’ by 0.05 increments until pedestal roughing pump kicks into action (the pump will become noticeably less grumbly at this crossover)
   (a) Continue increasing periodically so that temperature steadily falls $\sim$1 mK/sec
   (b) Should reach 2.2 K when ‘upper limit’ $\sim$ 2.25 or 2.3

While Cooling

1. Turn on (plug in) laser so that it can reach steady output voltage or wattage
   (a) Place black paper or other opaque device in front of laser so that it does not add unnecessary heat to helium system
2. Turn on camera power supply and open WinView32 or ImageJ camera software so that CCD may begin cooling
   (a) Ensure that the shutter is *closed*
   (b) Open ’Detect System Temperature’ to check that the CCD is indeed cooling
   (c) Temperature lock should be set to $T = -70°$C
   (d) No acquisition mode (’Focus’ nor ’Acquire’) should be activated until the temperature has been achieved and locked for at least 20 minutes
3. Check that the computer has enough free memory (usually > 60 GB to be safe)
4. Create injection mixture (See Section A.2 for procedure)

Prepare for Rotation

1. Make sure mixture bottle is full ($\sim$350 psi)
2. Disconnect copper tubing gas lines from rotating apparatus. Secure safely out of range of the rotating system.
3. Turn on air bearing

4. Turn on small, tuneable motor power supply. Set 'Output Voltage/Current' to *Off*
5. Turn on 120 V motor power supply
6. Check motor belt tension
7. Ensure that area around the rotating apparatus (beneath the rotating optical table, near the rotary vacuum unit, etc.) is clear

A.2 Creating He:H_2 Injection Mixture

NOTE: These directions create a 50:1 He:H_2 mixture.

1. Close all copper gas line valves
2. Attach trash bag to plastic white mixture nozzle
3. Open turquoise regulator ('Increase' all the way in)
4. Open trash bag valve to vent any residual mixture from silver bottle into trash bag
5. Open hydrogen copper gas line valves (2 knobs)
   (a) Do not open any solenoids via Matlab! These go to the cryostat!
6. Turn on hydrogen gas
   (a) On, gauge, then regulator until pressure reads $\sim$10 psi on the left mixture gauge
7. Open and close trash bag valve several times to flush lines and bottle with hydrogen gas
8. Turn off hydrogen gas
9. Open trash bag valve to vent remaining hydrogen from copper lines into trash bag
   (a) Now have 1 atm (14.7 psi) of hydrogen in bottle

(b) Copper tubing should be empty of hydrogen

(c) Mixture gauge should read zero

10. Close bottom hydrogen copper gas line valve (on optical table)

    (a) Leave upper valve (on rotating table) open

11. Open helium copper gas line valve (on optical table)

12. Turn on helium gas

    (a) Turn on main, then gauge, and then increase regulator until left mixture gauge reads 30 psi (red #s)

13. Vent 30 psi of helium gas into trash bag

    (a) Now have 2:1 He:H_2 mixture (30 psi : 15 psi)

14. Increase helium regulator until left mixture gauge reads 350 psi

15. Close all gas line valves

    (a) Mixture gauge should remain at 350 psi

    (b) Close (decrease) turquoise regulator

16. Empty copper lines of gas by opening (then closing) trash bag valve

17. Cap trash bag with thumb and release gas outside

18. Reopen turquoise regulator so mixture gauge reads $\sim$20 psi (first red dash)

Calculation for Injection Mixture

We present an example calculation for a 100:1 He:H_2 mixture as well as an explanatory example for very dilute mixtures.

We can describe the gases in the mixture using the ideal gas law, $PV = nRT$; however, since the volume V, the ideal gas constant R, and the temperature of the gas

T are all constant to first order, we can say that the pressure P scales linearly with the number of moles of gas n or $P \sim n$. Using this relationship, we can approximate the ratio of hydrogen to helium gas in the mixture by tabulating the relative number of moles of each gas. For example, if we begin with a bottle filled with hydrogen gas at 1 atm or $\sim$15 psi relative to "absolute zero" pressure and add 45 psi *above* atmosphere (i.e. $\sim$3 atm or 60 psi relative to absolute 0 psi) of helium gas, then we are left with a 3:1 mass ratio of helium to hydrogen. In other words, we have

$$1\,H_2 + 3\,He = 4\;Total$$

Normalizing, we obtain

$$\frac{1}{4}H_2 + \frac{3}{4}He = 1\;Total$$

If we equilibrate the 3:1 mixture with atmosphere (by "venting" or opening and closing the mixture valve), the ratio remains unchanged. Now, if we add 350 psi above atmosphere (or 365 psi relative to zero), then the ratio becomes

$$\frac{1}{4}H_2 + \left(\frac{3}{4} + \frac{365}{15}\right)He = 1 + \frac{365}{15}$$

From here, it is simple to calculate mass fractions; we have $\sim$99% helium and correspondingly, $\sim$1% hydrogen.

The formula for finding the mixture ratio given two pressure values is thus

$$\frac{f_{H_2}}{(1 - f_{H_2}) + \frac{p_{abs}}{15}}$$

where f_{H_2} is the fraction of hydrogen gas in the bottle after the first helium gas addition

and p_{abs} is the absolute pressure of helium gas added to the bottle after that (Gauge pressure = $p_{abs} - 15$).

Given the values above where $f_{H_2} = 1/4$ and $p_{abs} = 365$, we find a mixture ratio of approximately 100:1 He:H_2.

To create very dilute mixtures, it is easiest to simply fill the mixture bottle with 1 atm ($\sim$15 psi absolute pressure) of hydrogen gas and then add 350 psi (365 absolute pressure) of helium gas. Consider

1 unit of H_2 (15 psi absolute)

23 units of He (365 psi absolute)

24 total units

Then,

$$\frac{1}{24} H_2 + \frac{23}{24} He = 1$$

Opening and closing the mixture valve is essentially equivalent to equilibrating this mixture with atmosphere and then filling with another 23 units of He. Thus, we have

$$\frac{1}{24} H_2 + \left(\frac{23}{24} + 23 \right) He = 1 + 23$$

or rather

$$\frac{1}{(24)^2} H_2 + \left[\frac{23}{(24)^2} + \frac{23}{24} \right] He = 1$$

Another 23 units of helium gas gives us

$$\frac{1}{(24)^3} H_2 + \left[\frac{23}{(24)^3} + \frac{23}{(24)^2} + \frac{23}{24} \right] He = 1$$

which is a lovely example of a geometric series. Conveniently, we can now write the helium fraction as

$$\text{He: } 1 - \frac{1}{24^v}$$

were v is the number of times 23 units of helium are added to the mixture (or "vented").

The mass fraction of hydrogen to helium is then simply

$$\frac{1/24^v}{1 - 1/24^v}$$

A.3 Cooling the System from Very Hot (> 200 K) Temperatures

After a full day of running liquid helium experiments, there two main reasons the cryostat is excessively hot the following morning:

1. Little or no liquid helium was left in the cryostat at the end of the previous day's run.
2. The vacuum jacket is corrupted.

The first reason has an easy solution: leave a little bit of liquid helium in both the test and bath sections before closing up for the day. Generally leaving the test section full to just past the windows and the bath section 15-20% full will ensure a cool cryostat the following day.

A bad vacuum jacket is a much more vexatious problem. While cryopumping will maintain a quality vacuum as long as there is liquid helium in the system (or as long as inner walls of cryostat are below 77 K), as soon as that is gone, the temperature will spike and rapidly increase. Thus, even if the preventive measures are taken to leave

the cryostat well-filled with liquid helium at the end of the day, the steep temperature gradient will likely counteract these measures as soon as the helium has boiled away.

To cool the system from temperatures above 200 K, follow the standard operating procedures (Section A.1) until liquid helium begins accumulating in the system (see page 70). It is likely that there will be a slight sputtering sound coming from the brass nozzle, indicating that liquid helium is trying to form. Likewise, the helium level sensor will begin to give values greater than -1.0 (even if they are still negative). Then, open the side test section port to encourage excess (i.e. boiled off) gas out of the port. It is important to make sure that gas is always flowing *out* of the port! This procedure results in a significantly less isothermic system, but dramatically speeds up the cooling process.

While the side port is open, one may close the bath section valve partially to encourage more helium to flow into the test section (thereby cooling it) even faster. Then, when the temperature in the test section is < 100 K, heat, clean, and recap test section side port. This step must be done well before temperature "drop off" (specific heat change) $\sim$40 K. Finally, fully reopen bath section valve, and continue with the directions in Section A.1.

A.4 Apparatus Rotation Rate

See Fig. A.1.

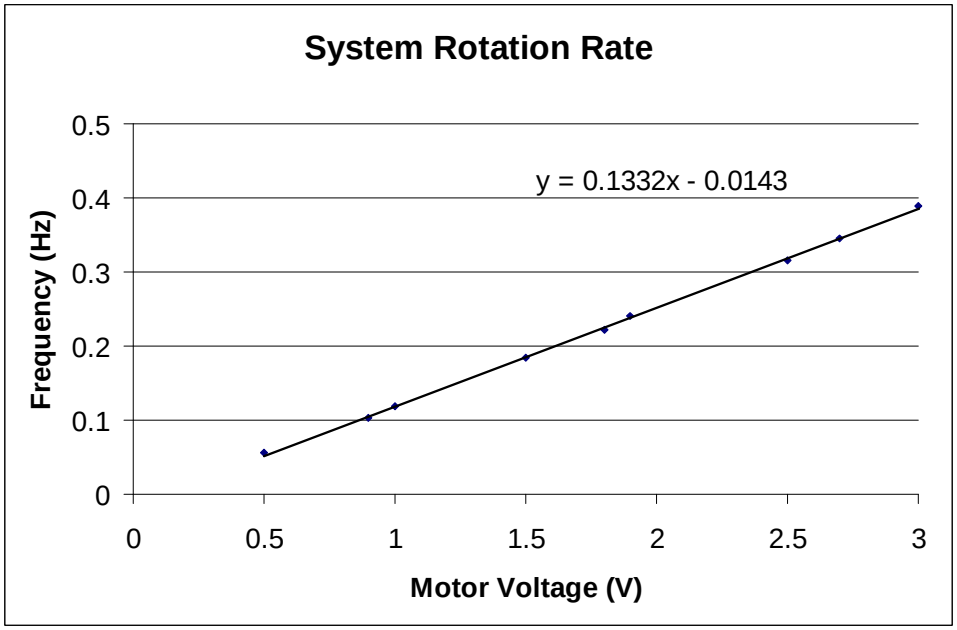

Figure A.1: System rotation rate as a function of motor input voltage

Bibliography

[1] H. K. Onnes. The liquefaction of helium. *Koninklijke Nederlandsche Akademie van Wetenschappen Proceedings (Proc. R. Netherlands Acad. Arts Sci.)*, 11:168, 1908.

[2] D. van Delft. Little cup of helium, big science. *Physics Today*, p.36-42, March 2008.

[3] Science and Its Times: Understanding the Social Significance of Scientific Discovery, ed. by Neil Schlager, 7 vols. (Chicago: Gale Group, 2000-2001), Vol. VI, 430-432.

[4] H. K. Onnes. On the sudden change in the rate at which the resistance of mercury disappears. *Comm. Leiden.*, 12:120, 1911.

[5] H. K. Onnes. Investigations in the properties of substances at low temperatures, which have led, amongst other things, to the preparation of liquid helium. Nobel Lecture, Dec. 11, 1913.

[6] H. K. Onnes and J. D. A. Boks, *Comm. Leiden*, 170b, 1924.

[7] W. H. Keesom and M. Wolfke. The two different liquid states of helium. *Leiden Comm.*, 190b, 1927.

[8] W. H. Keesom and M. Wolfke. On the change of the dielectric constant of liquid helium with temperature. Provisional measurements. *Proc. Acad. Sci. Amsterdam*, 31:81, 1928.

[9] W. H. Keesom and M. Wolfke. *Proc. Acad. Sci. Amsterdam*, 31:90, 1928.

[10] W. H. Keesom and J. N. van der Ende. *Proc. Roy. Ac. Amsterdam*, 33:24, 1930.

[11] W. H. Keesom and K. Clusius. *Proc. Acad. Sci. Amsterdam*, 35:307, 1932.

[12] W. H. Keesom and A. P. Keesom. *Proc. Acad. Sci. Amsterdam*, 35:736, 1932.

[13] Parenteel van Johann Bernard Theodorus Moormann. Retrieved 13 May 2010 from http://www.jhmoormann.nl/bomen/holland.HTML.

[14] J. C. McLennan, H. D. Smith, and J. O. Wilhelm, *Phil. Mag.*, 14:161, 1932.

[15] W. H. Keesom, *Proc. Acad. Sci. Amsterdam*, 36:147, 1933.

[16] J. O. Wilhelm, A. D. Misener, and A. R. Clark. The Viscosity of Liquid Helium. *Proc. Roy. Soc. (London)*, A151:342, 1935.

[17] E. F. Burton. Viscosity of helium I and helium II. *Nature*, 135:265, 1935.

[18] A. Griffin. The Discovery of Superfluidity: A Chronology of Events in 1935-1938. 2006. Extended version of A. Griffin. Superfluidity: three people, two papers, one prize. *Physics World*, August 2008.

[19] W. H. Keesom and A. P. Keesom. On the heat conductivity of liquid helium. *Physica*, 3:359, 1936.

[20] J. F. Allen, R. Peierls, and M. Z. Uddin. Heat Conduction in Liquid Helium. *Nature*, 140:62, 1937.

[21] BBC Documentary: Absolute Zero, The Conquest of Cold. First broadcast on 24 Jul 2007.

[22] R. J. Donnelly and C. F. Barenghi. The Observed Properties of Liquid Helium at the Saturated Vapor Pressure. *J. Phys. Chem. Ref. Data*, 27:1217–1274, 1998.

[23] J. F. Allen and A. D. Misener. Flow of Liquid Helium II. *Nature*, 141:75, 1938.

[24] P. Kapitsa. Viscosity of Liquid Helium below the λ-Point. *Nature*, 141:74, 1938.

[25] J. F. Allen and H. Jones. New Phenomena Connected with Heat Flow in Helium II. *Nature*, 141:243, 1938.

[26] A. Chodos (Editor). This Month in Physics History – January 1938: Discovery of Superfluidity. *APS News*, Vol. 15, No. 1, January 2006.

[27] J. G. Daunt and R. S. Smith. The Problem of Liquid Helium. *Rev. Mod. Phys.*, 26:1, 1954.

[28] J. Mehra and H. Rechenberg. *The Conceptual Completion and the Extensions of Quantum Mechanics*. Vol. 6, p.869-877. Springer-Verlag, New York, 2001.

[29] L. Tisza. Transport Phenomena in Helium II. *Nature*, 141:913, 1938.

[30] J. G. Daunt and K. Mendelssohn. Surface transport in liquid helium II. *Nature*, 143:719, 1939.

[31] L. D. Landau. Theory of the Superfluidity of Helium II. *Phys. Rev.,* 60:356, 1941.

[32] R. J. Donnelly. *Quantized Vortices in Helium II.* Cambridge Univ. Press,

Cambridge, UK, 1991.

[33] G. P. Bewley. *Using frozen hydrogen particles to observe rotating and quantized flows in liquid helium.* Ph.D. thesis, Department of Mechanical Engineering, Yale University, New Haven, CT USA, 2006.

[34] M. S. Paoletti. *Experimental Characterization of Turbulent Superfluid Helium*. Ph.D. thesis, Department of Physics, University of Maryland, College Park, MD USA, 2010.

[35] R. P. Feynman. Applications of quantum mechanics to liquid helium. In C. J. Gorter, editor, *Prog. in Low Temp. Phys.*, 1:17–53, Amsterdam, 1955.

[36] Tornadoes. Wikipedia. Retrieved 12 May 2010 from http://www.nssl.noaa.gov/headlines/dszpics.html

[37] G. A. Williams and R. E. Packard. Photographs of quantized vortex lines in rotating He II. *Phys. Rev. Lett.* 33(5):280-283, 1974.

[38] E. J. Yarmchuk, M. J. V. Gordon, and R. E. Packard. Observation of Stationary Vortex Arrays in Rotating Superfluid Helium. *Phys. Rev. Lett.*, 43:214– 217, 1979.

[39] G. P. Bewley, D. P. Lathrop and K. R. Sreenivasan. Superfluid helium: visualization of quantized vortices. *Nature* 441:588-589, 2006.

[40] J. R. Abo-Shaeer, C. Raman, J. M. Vogels, and W. Ketterle. Observation of Vortex Lattices in Bose-Einstein Condensates. *Science*, 292:476–479, 2001.

[41] U. Essmann and H. Träuble. The Direct Observation of Individual Flux Lines in Type II Superconductors. *Physics Letters*, 24A:526-527, 1967.

[42] W. H. Zurek. Cosmic Strings in Laboratory Superfluids and the Topological Remnants of Other Phase Transitions. *Acta Physica Polonica B*, 24(7):1301-1311, 1993.

[43] P. G. de Gennes and J. Prost. *The Physics of Liquid Crystals*. Second edition. Oxford Univ. Press, Oxford, UK, 1993.

[44] H. E. Hall and W. F. Vinen. The Rotation of Liquid Helium II. Proc. of the Royal Soc. of London. 238A(1213):215-234, 1956.

[45] V. K. Tkachenko. Stability of Vortex Lattices. *Soviet Phys JETP*, 23:1049, 1966.

[46] E. B. Sonin. Vortex oscillations and hydrodynamics of rotating superfluids. *Rev. Mod. Phys.* 59(1):87-155, 1987.

[47] I. Coddington, P. Engels, V. Schweikhard, and E. A. Cornell. Observation of

Tkachenko Oscillations in Rapidly Rotating Bose-Einstein Condensates. *Phys. Rev. Lett.*, 91:10, 2003.

[48] C. D. Andereck *et al*., *Phys. Rev. Lett.*, 1979.

[49] C. D. Andereck and W. I. Glaberson. Tkachenko Waves. *Journal Low Temp. Phys*, 48:3-4, 1982.

[50] R. J. Donnelly. Theory of the Interaction of Ions and Quantized Vortices in Rotating Helium II. *Phys. Rev. Letters*, 14:39, 1965.

[51] M. Paperin. Introduction to Cloud Structures. Hamburg, Germany, May 2007

[52] K. Stewartson. On almost rigid rotations. Part 2 Journal of fluid mechanics, 26(1):131-144, 1966.

[53] D. Fultz, R. R. Long, G. V. Owens, W. Bohan, R. Kaylor, and J. Weil. Studies of Thermal Convection in a Rotating Cylinder with Some Implications for Large-Scale Atmospheric Motions. *Meteor. Monogr*. 4(21), 1959.

[54] M. S. Paoletti, R. B. Fiorito, K. R. Sreenivasan, and D. P. Lathrop. Visualization of Superfluid Helium Flow. *J. Phys. Soc. Japan*, 77(11):111007, 2008.

[55] J. K. Hunter, J.-M. Vanden-Broeck. Solitary and periodic gravity-capillary waves of finite amplitude. *J. Fluid Mech.* 134:205–219, 1983.

[56] J. M. Lattimer and M. Prakash. The Physics of Neutron Stars. *Science*, 304:536, 2004.

[57] A. Melatos, C. Peralta, and J. S. B. Wyithe. Avalanche Dynamics of Radio Pulsar Glitches. *The Astrophys. Jour.*, 672:1103, 2008.

[58] C. Peralta and A. Melatos. An Unstable Superfluid Stewartson Layer in a Differentially Rotating Neutron Star. *The Astrophys. Jour.*, 701:L75-L78, 2009.

[59] I. F. Sbalzarini and P. Koumoutsakos. Feature Point Tracking and Trajectory Analysis for Video Imaging in Cell Biology, Journal of Structural Biology 151(2):182-195, 2005.